A Multi-site Passive Approach for Studying the Emissions and Evolution of Smoke from Prescribed Fires

Rime El Asmar[1], Zongrun Li[2], David J. Tanner[1], Yongtao Hu[2], Susan O'Neill[3], L. Gregory Huey[1], M. Talat Odman[2], Rodney J. Weber[1]

[1]School of Earth and Atmospheric Sciences, Georgia Institute of Technology, Atlanta, 30331, USA.
[2]School of Civil and Environmental Engineering, Georgia Institute of Technology, Atlanta, 30331, USA.
[3]USDA Forest Service, Pacific Northwest Research Station, 400 North 34th Street, Suite 201, Seattle, WA 98103, USA.

Correspondence to: Rodney J. Weber (*rweber@eas.gatech.edu*)

Abstract. We conducted a two-year study utilizing a network of fixed sites with sampling throughout an extended prescribed burning period to characterize the emissions and evolution of smoke from silvicultural prescribed burning at a military base in the southeastern US. The measurement approach and an assessment of instrument performance is described. Smoke sources, including those within and off the base, are identified, and plume ages are determined to quantify emissions and study the evolution of smoke $PM_{2.5}$ mass, black carbon (BC), and brown carbon (BrC). Over the 2021 and 2022 prescribed burning seasons (nominally January to May), we identified 64 smoke events based on high levels of $PM_{2.5}$ mass, BC, BrC, and carbon monoxide (CO), of which 61 were linked to a specific burning area. Smoke transport times were estimated using the mean wind speed along with the distance between fire and measurement site, and with HYSPLIT back trajectories. $PM_{2.5}$ emission ratios based on $\Delta PM_{2.5}$ mass/ΔCO for fresh smoke (age $\leq$ 1 hour) ranged between 0.04 and 0.18 $\mu g\ m^{-3}\ ppb^{-1}$ with a mean of 0.117 $\mu g\ m^{-3}\ ppb^{-1}$ (median of 0.121 $\mu g\ m^{-3}\ ppb^{-1}$). Both the mean emission ratio and variability were similar to findings from other prescribed fire studies, but lower than wildfires. Mean emission ratios of BC and BrC were 0.014 $\mu g\ m^{-3}\ ppb^{-1}$ and 0.442 $Mm^{-1}\ ppb^{-1}$ respectively. Ozone enhancements (ΔO_3) were always observed in plumes detected in the afternoon. $\Delta PM_{2.5}$ mass/ΔCO was observed to increase with plume age in all ozone enhanced plumes suggesting photochemical secondary aerosol formation. In contrast, $\Delta BrC/\Delta CO$ was not found to vary with plume ages less than 8 hours during photochemically active periods.

1. Introduction

Large and intense wildfires have been increasing over the past few decades and their emissions are a critical concern (Singleton et al., 2019; Jaffe et al., 2020). Fire is also an essential ecological process and prescribed burning, which is the act of starting controlled fires for specific purposes, is an important tool for restoration of ecosystems, land management, and reducing fuel to prevent destructive wildfires (Kelp et al., 2023). Prescribed fires are typically conducted during favorable conditions associated with the fuel type and amount, soil moisture, and meteorology. For example, in 2018, the United States Department of Agriculture (USDA) Forest Service indicated a high risk of hazardous wildfires over approximately 234 million acres (~ 95 million ha) of forest lands in the US (Wyden and Manchin, 2020). However, prescribed fires were conducted over approximately 8.5 million forestry/rangeland acres (3.4 million ha) in 2018 (Melvin, 2020). The southeastern US has a long history of using prescribed fires (Melvin, 2021). For example, in 2017, 7.6 million acres (3 million ha) out of the 11.3 million acres (4.6 million ha) burned nationally were in the southeast (Melvin, 2018). Florida and Georgia each exceeded 1 million acres (0.4 million ha) burned annually (Melvin, 2018). Recognizing the need to mitigate the size and severity of wildfires, prescribed burning is anticipated to increase in the coming years (USDA, 2022).

While prescribed burning can be performed under favorable weather conditions, it can still contribute to serious local and regional air pollution as it is a source of primary and secondary air pollutants (Lee et al., 2008). Like other types of biomass burning, prescribed burning releases large amounts of particulate matter, CO, and inorganic and organic compounds (Lee et al., 2005), which have negative effects on health and visibility (Bell, 2004; Huang et al., 2019). Particularly in the southeastern US, prescribed burning was significantly associated with high $PM_{2.5}$ levels (Afrin and Garcia-Menendez, 2020; Larkin et al., 2020). Prescribed fires are often conducted at urban-rural interfaces creating a buffer zone to prevent the spread of wildfires towards the built environment. However, this means that the planned fires often occur closer to populated areas, and potentially lead to high population exposure due to this proximity. Although prescribed fires generally produce less pollutants by consuming less fuel per area burned than wildfires, the population health costs can be substantially higher for prescribed fires due to burning near higher population densities (Borchers-Arriagada et al., 2021).

Both wildfires and prescribed fires emit a large variety of gases and particulates (Liu et al., 2017b; Burling et al., 2011; Gkatzelis et al., 2024; Permar et al., 2021; Travis et al., 2023). Gases include nitrogen oxides and volatile organic compounds that can form ozone and secondary particulate matter. Hazardous air pollutants are also produced but they may be less detrimental to exposed populations than particulates (O'Dell et al., 2022). $PM_{2.5}$, (particulate matter with aerodynamic diameter of 2.5 micrometers or smaller), is directly emitted as primary particles and also formed from condensation of emitted gases and their oxidation products (Liu et al., 2016; May et al., 2014). While secondary organic aerosol (SOA) can be a significant component of aged biomass burning $PM_{2.5}$, its contribution changes depending on emissions and atmospheric conditions. Additionally, the volatile nature of primary and secondary components of $PM_{2.5}$ can lead to evaporation and a net loss in mass as the plume ages. $PM_{2.5}$ exposure has been linked in many epidemiological studies to serious health problems such as respiratory, cardiovascular, and neurological diseases, as well as increased risk of adverse birth outcomes (Liu et al., 2015; Reid et al., 2016; Naeher

63   et al., 2007; Yu et al., 2023; Xi et al., 2020; Garcia et al., 2023). Given their significant impact on the environment

64   and health, satellite, airborne, or ground-based studies of smoke emissions have been extensively conducted.

65   Detection and characterization of wildland fires is an important step towards assessing their impacts. Remote

66   sensing via satellites can detect wildland fires by thermal anomalies (Kuenzer et al., 2008) or vegetation changes

67   (Mildrexler et al., 2007). While satellite-based approaches offer valuable insights (Martinsson et al., 2022; Ichoku and

68   Kaufman, 2005; Christopher et al., 1998), challenges such as cloud cover, spatial resolution limitations, and the

69   complex nature of fire emissions can hinder accurate detection and quantification of fire impacts, especially for lower-

70   intensity fires like prescribed burns (Liu et al., 2019; Wang et al., 2018; Martin et al., 2018). Therefore, factors like

71   Fire Radiative Power (FRP), burned area estimation, and fuel consumption modeling are often integrated into fire

72   monitoring systems (Li et al., 2020; Nguyen and Wooster, 2020).

73   Aircraft (fixed wing and helicopters) and more recently drones are commonly used in airborne studies of

74   wildland fires (Decker et al., 2021b; Cubison et al., 2011; Aurell and Gullett, 2024) and have been deployed for

75   prescribed burning studies (Yokelson et al., 1999; May et al., 2014; Pratt et al., 2011; Aurell et al., 2021). Airborne

76   studies provide high spatial resolution data that are often used to assess evolution of smoke properties by

77   measurements at various downwind distances, however, it is non-continuous, and can miss certain aspects of smoke

78   emissions, such as longer-term smoldering, especially at night (Burling et al., 2011). Employing a combination of

79   airborne and ground-based measurements can be beneficial in providing a comprehensive view of the plume (Burling

80   et al., 2011; Akagi et al., 2014; Yokelson et al., 2013; Strand et al., 2016).

81   In ground-based studies, mobile labs may capture dynamic air quality patterns and to some extent assess

82   spatial variability of species in plumes and their changes with plume age (Levy et al., 2014; Fiddler et al., 2024; Lee

83   et al., 2023). However, they are usually limited in space and instrumentation capacity, such as filter samples collected

84   only during stationary measurements (Warneke et al., 2023). Interferences from the power source, vibration and speed

85   changes during transportation can affect instrument stability and performance leading to inaccurate measurements or

86   limiting the type of instruments that can be used. Attempting to track wildland smoke plumes can be challenging due

87   to unpredictable winds and dispersion conditions combined with access limitations. For example, Burling et al. reports

88   successfully sampling smoke from 2 out of 14 prescribed fires using a battery powered mobile FTIR system (Burling

89   et al., 2011).

90   Fixed ground-based monitoring stations equipped with various instruments provide continuous, localized

91   measurements for short or long-term monitoring for studies assessing diurnal, seasonal, and long-term trends in air

92   pollution. Multiple sites provide spatial coverage within a region. A variety of highly sensitive instruments can be

93   deployed, ensuring accurate and precise measurements of various pollutants that can be compared with air quality data

94   across different locations for regional assessments (Strand et al., 2016; Warneke et al., 2023). The importance of pre-

95   existing fixed monitoring sites lies in their ability to capture wildfire smoke events that can occur at any time

96   (Selimovic et al., 2019; Jaffe et al., 2022). These sites often include regulatory monitoring stations, which are highly

97   valuable for studying local and regional smoke impacts over both short and long-term periods. For example, Jaffe et

98   al. used $PM_{2.5}$ and CO observations from a regulatory monitoring site in Sparks, NV, collected from May to September

99   between 2018 and 2021, as indicators of wildfire smoke in urban areas (Jaffe et al., 2022). Investigating emissions

100 and evolution of prescribed fires based on fixed sites is not as common, and there are limitations with this approach,
101 but also some advantages.

102   Here, we present results from a two-year study utilizing fixed monitoring stations and continuous sampling
103 in a region of active prescribed burning at Fort Moore in central Georgia, USA. The observations are analyzed to
104 identify smoke plumes and determine their sources, such as those set within the Fort or from burning in surrounding
105 areas. We also use these data to estimate the age of the smoke detected to determine emission ratios and changes with
106 plume age of $PM_{2.5}$ mass, BC, and BrC and their variability. Not all smoke from the prescribed fires set within the
107 Fort are detected so the overall impact of all fires on regional air quality cannot be determined and is better addressed
108 by a model simulation. Instead, our goal is to sample multiple smoke events so that an analysis of the data will provide
109 a robust characterization of smoke from prescribed burning within the Fort and in the region and sufficient data to
110 evaluate ground-level pollutant concentrations predicted by "smoke" models in prescribed fire simulations. Our
111 concentration data cover measurements over a large range of distances from the burn plots. Fresh plume measurements
112 with ages less than 1 hour can be used in evaluating the predictions of local scale models such as the Wildland urban
113 interface Fire Dynamics Simulator (WFDS) (Mell et al., 2007) and the QUIC-Fire (Linn et al., 2020). They can also
114 be used in evaluating the emissions and plume-rise parameterizations of larger scale models like the BlueSky
115 framework (Larkin et al., 2009). Additionally, more aged smoke measurements can be used to test the predictions of
116 downwind concentrations in coupled fire-atmosphere models such as WRF-SFIRE (Mandel et al., 2011) as well as
117 chemical transport models like the Community Multiscale Air Quality (CMAQ) model (Appel et al., 2021), when they
118 are equipped with fire plume parameterizations. In the following sections, we describe the methodology, data analysis
119 approach, case studies of various detected or missed smoke plumes so that attribution of smoke from fires within the
120 Fort can be assessed. Findings on emission estimates of $PM_{2.5}$ mass, BC, and BrC and their evolution are compared
121 to other prescribed and wildfire studies. These findings can help to assess the impact of prescribed burns by a specific
122 entity or organization on a variety of public health and policy issues.

123   **2. Method**

124   **2.1. Site description**

125   Prescribed burning at Fort Moore Army Base, (formerly Fort Benning), in west central Georgia, United
126 States, was studied during March through May of 2021 and February through May of 2022. Since 1981, prescribed
127 burning has been used as a land management tool at the 182,000 acres (~ 74, 000 ha) military base, of which 145,000
128 acres (~ 59,000 ha) are forested lands. Vegetation is characterized by pine-dominated uplands and hardwood-
129 dominated bottomlands, with the dominant tree species being longleaf pine and white oak, respectively. Small
130 wildfires ignited during military training exercises also occur at the base and the land managers have been recording
131 data on both prescribed fires and wildfires since the 1980s. Prescribed burning at the Fort has been effective; it has
132 reduced the frequency of wildfires from ~ 300-500 wildfires/year in the early 1980s to less than 100 wildfires/year in
133 the mid-1990s. During this period the prescribed fire burnt area changed from ~7,500 acres (~ 3,000 ha) in 1981 to ~
134 12,000 acres (~ 5,000 ha) in 1992. Currently, 30,000 woodland acres (~ 12,000 ha) are burned annually using

135   controlled fires, with a future planned burning of 45,000 acres (~ 18,000 ha) annually. Prescribed burning on the Fort

136   is also used for ecological objectives, such as restoring the longleaf pine forest and creating and maintaining habitat

137   for red-cockaded woodpeckers. Prescribed burning occurs from December through May when there is sufficient but

138   not excessive rainfall, and suitable temperatures and wind conditions to burn deadwood, brush, and low-growing

139   vegetation accumulating on the forest floor. The area of the base is divided into 332 burn units that range in size from

140   100 to 1,800 acres (~ 40 to 728 ha) and are burnt alternately every two to three years.

141   **2.2. Measuring sites**

142   One instrumented research trailer (7'W x 18'L x 6.5'H) was deployed in the 2021 burning season (March 18,

143   2021 to May 15, 2021), and successively trailers (6'W x 12'L x 7'H) were added in 2022 (February 11, 2022 to May

144   18, 2022) reaching a total of five trailers located at different sites throughout the Fort. In 2021, the one trailer operated

145   at the same location until it was moved on April 26, 2021 to a new site for the remaining season as expected burning

146   regions at the Fort changed. The trailers sampled continuously, except during periods of power loss or technical issues.

147   The locations of trailers, shown in Fig. 1, were chosen based on power availability, prevailing wind, and burning plans

148   set prior to the burning season.

149   **2.3. Instrumentation**

150   To characterize the prescribed fire smoke, the trailers were equipped with several instruments selected based

151   on factors such as availability, ability for extended stand-alone operation, and their significance to the study. All

152   sampling was done through inlets nominally 4 m above ground level and 1.5 m above the trailer roof. Measurements

153   included, carbon monoxide (CO), nitrogen oxides (NO, NO_2, NO_x), ozone (O_3), $PM_{2.5}$ mass concentration and black

154   carbon (BC) concentration and brown carbon (BrC) light absorption coefficients. Carbon monoxide serves as a

155   standard tracer for combustion sources in atmospheric chemistry studies since it is a relatively long-lived species, with

156   a typical lifetime of ~ 1 month, emitted during incomplete combustion and used as a tracer of smoke movement and

157   dispersion (Forrister et al., 2015; Liu et al., 2016). Other forms of incomplete combustion emissions (e.g., mobile

158   sources) and oxidation of VOCs are also CO sources. CO mixing ratios were measured by IR analyzers (Thermo

159   Fisher Scientific Inc, model 48C, Franklin, MA) with a lower detection limit (LOD) of 0.04 ppm at an averaging time

160   of 390 seconds. The measurements alternated between blank and ambient measurements every 195 seconds. The

161   blanks were determined with a custom-built CO scrubber made of 0.5 % Pd on alumina catalyst heated to 180 °C

162   (Parrish et al., 1994), which oxidizes CO to CO_2. Calibration of CO analyzers was performed at 2.2 ppm concentration

163   before and after each field study using a 100 ppm CO in air standard purchased from nexAir (Memphis, TN).

164   O_3 was measured using an ultraviolet (UV) photometric analyzer (Thermo Fisher Scientific Inc, model 49C,

165   Franklin, MA) zeroed through an O_3 scrubber in the instrument, with LOD of 1.0 ppb and averaging time of 20

166   seconds. The analyzer was calibrated before and after each field deployment using an O_3 calibrator (Thermo Fisher

167   Scientific Inc, model 49C, Franklin, MA). We note that O_3 may be overestimated due to interferences from VOCs

168   emitted by the fire (Long et al., 2021), but the instrument used has been found to be in agreement with a federal

169   reference method (Gao and Jaffe, 2017). NO_x species were measured using a chemiluminescence NO-NO_2-NO_x

170 analyzer (Thermo Fisher Scientific Inc, model 42i, Franklin, MA). The NO_x analyzer was calibrated automatically

171 every 6 hours, using NO and NO_2 calibration standards purchased from Airgas (Radnor, PA) and has an LOD of 0.40

172 ppb.

173 PM$_{2.5}$ mass concentration was determined with a Tapered Element Oscillating Microbalance (TEOM) series

174 1400a ambient particulate monitor (Thermo Fisher Scientific, Franklin, MA) with data recorded at an averaging time

175 of 60 seconds and typical detection limit of 5.58 μg m^{-3} determined by 3 standard deviations of blank (filtered ambient

176 air) measurements. This data was subsequently averaged to time intervals of 20 and 60 minutes to mitigate noise,

177 especially when sampling under background conditions. The TEOM series 1400a developed originally by Rupprecht

178 & Patashnick is a US-EPA approved instrument for measuring the mass concentration of ambient PM$_{2.5}$ and PM$_{10}$ and

179 could be used for Federal Equivalent Method (FEM) regulatory measurements (Liu et al., 2017a; Patashnick and

180 Rupprecht, 1991). It is a gravimetric measurement that determines the mass accumulated on a microbalance over a

181 specified time interval at a monitored sample air flow rate. The sample air is preconditioned to a temperature of 50 °C

182 to remove liquid water interferences (Patashnick and Rupprecht, 1991), which may lead to the evaporation of highly

183 volatile PM$_{2.5}$ components, potentially underestimating the total mass concentration. Mass concentration over an

184 averaging period is calculated from the difference recorded between successive intervals. Due to random fluctuations

185 in the instrument operation when concentrations are low, this can lead to negative numbers, illustrated by the frequency

186 distribution of high time resolution data recorded by one TEOM shown in Fig. S1. When determining the average

187 background concentration, we include the negative mass concentrations since converting negative concentrations to

188 one half the LOD or ignoring them will produce an average that is biased high. In 2021, PM$_{10}$ TEOMs were also

189 deployed but this was found to be highly influenced by pollen, which can be high in the springtime, and so the

190 measurement was discontinued. Regional hourly PM$_{2.5}$ mass was reported at two Environmental Protection Division

191 (EPD) sites. In the following analysis we compare the PM$_{2.5}$ measured within the Fort to the EPD measurements at

192 the Columbus Airport and Phenix City South Girard (PCSG) school shown on the map in Fig. 1a. At Columbus

193 Airport, the Teledyne T640, which is based on broadline spectroscopy, is used, while the Met One BAM-1022 mass

194 monitor is used in Phenix City, utilizing a beta attenuation technique.

195 PM$_{2.5}$ black carbon (BC) mass concentration was measured by aethalometers. A range of multi and single

196 wavelength instruments were deployed. Two were seven wavelength instruments (Magee Scientific, model AE33 and

197 model AE31, Berkeley, CA) with detection ranges of 0.1–100 μg m^{-3} and averaging times of 60 and 120 seconds

198 respectively, one 2-wavelength aethalometer (Magee Scientific, model AE22, Berkeley, CA) of 0.1 μg m^{-3} detection

199 limit and 60 seconds averaging time, and two single wavelength particle soot absorption photometers (PSAPs)

200 (Radiance Research, Seattle, WA) of sensitivity > 0.1 μg m^{-3} for 60 seconds averaging time. For the multiwavelength

201 aethalometers, BC was determined from the light absorption at 880 nm using the manufacturer's specified mass

202 absorption cross-section (MAC) of 7.77 m^2 g^{-1}, whereas for the single wavelength PSAPs, BC was determined from

203 the optical absorption coefficient at 565 nm assuming a specific mass absorption cross-section of 10 m^2 g^{-1} following

204 the manufacturer's specifications. Two spot samplings of the model AE33 corrected for mass loading errors. This was

205 not done in the other instruments and so the data of the aethalometers (AE31 and AE22) were corrected for loading

206 interference using the method of Virkkula et al. (Virkkula et al., 2007). PSAPs measurements were not corrected due

207 to unavailability of scattering coefficients needed for correcting filter-based PSAP measurements (Bond et al., 1999;
208 Virkkula et al., 2005), which may lead to 10-20% underestimation of BC at sites where PSAPs were installed.

209   Brown carbon (BrC) was calculated from the 7-wavelength aethalometer measurements. BrC is largely
210 produced from biomass burning (Hecobian et al., 2010; Laskin et al., 2015; Yan et al., 2018; Fleming et al., 2020) and
211 in the following analysis used as a unique indicator of biomass burning smoke. While a small amount of BrC can be
212 produced from mobile sources and other sources of incomplete combustion, in the US, its predominant source is
213 biomass burning (Jo et al., 2016; Hecobian et al., 2010). We calculate the light absorption of BrC at 365 nm as a
214 marker for BrC levels. Using the aethalometer data, the absorption coefficient, which corresponds to (BC+BrC), was
215 inferred by multiplying mass concentration at each wavelength by the corresponding MAC value provided by the
216 manufacturer (Magee Scientific, Berkeley, CA). The absorption coefficient at 365 nm was determined by
217 extrapolating the linear regression of log absorption coefficient vs log wavelength since the lowest wavelength at
218 which the aethalometer operates is 370 nm. The slope of the linear relationship represents the negative of the
219 absorption Angstrom Exponent (AAE), a parameter used to study the optical properties of the aerosol. BrC at 365 nm
220 was then calculated by removing the estimated contribution of BC at 365 nm assuming that BrC does not absorb at
221 880 nm and that AAE of pure BC is 1. BrC absorption at shorter wavelengths is the difference of aethalometer-
222 measured total absorption and the extrapolated BC absorption (Lack and Langridge, 2013). All data of the light
223 absorption of BrC discussed in this work corresponds to the absorption calculated at 365 nm. Both AAE_{total} and AAE_{BrC}
224 were calculated as the negative slopes of log absorption coefficient of total (BC+BrC) and BrC respectively, as a
225 function of log wavelengths. For AAE_{total} the fit included wavelengths 370–880 nm (i.e., 370, 470, 520, 590, 660,
226 880), whereas for AAE_{BrC} the wavelengths ranged from 370 to 660nm (i.e., 370, 470, 520, 590, 660).

227   In our analysis, we used meteorological and fuel moisture data from the Remote Automated Weather Stations
228 (RAWS) available online (https://raws.dri.edu/index.html). The closest RAWS weather station to all sites is named
229 Ft. Benning Georgia (Fig. 1a). In each trailer, all instruments were connected to a laptop computer with remote access
230 to reduce personnel time spent at the sites. Sites were generally visited every 1 to 2 weeks during which regular
231 instrument checks and maintenance were performed, such as restoring power, changing filters (for TEOMs and
232 PSAPs), measuring and recording flow rates and other instrument performance parameters.

2.4. Tools and analysis methods

2.4.1. Normalized Excess Mixing Ratios

235   To account for dilution of species of interest in a smoke plume, Normalized Excess Mixing Ratios (NEMRs)
236 are used. The NEMR is the ratio of enhancement of a studied species above the local background concentrations to
237 the enhancement of a long-lived component co-emitted from the biomass burning event. CO is often used as the
238 reference species, i.e., NEMR of species X is $\Delta X/\Delta Y$, where Y is CO measured in the same sample as X. To determine
239 the NEMR of X and the contribution of smoke to X from an identified burning region, the background concentration
240 of X (i.e., concentration if no smoke emissions) is subtracted from the measurement. In our study we used the average
241 of the measurements before and after the smoke event as the background since sampling was not performed upwind
242 of the fire. This method is supported by the observation from multiple sampling sites of spatially uniform background

243 concentrations and, in most cases, very low background concentrations relative to those recorded in the smoke.
244 However, there is more uncertainty when calculating O_3 NEMRs due to significant levels and diurnal changes in
245 background concentrations. NEMRs can also be determined from the slope of linear regressions. Here, we determine
246 NEMRs in each smoke event for $PM_{2.5}$ mass, BC, and BrC normalized by CO by first removing background
247 concentrations for data recorded during the event and then calculating the slope by linear regressions (i.e., the slope
248 of $PM_{2.5}$ mass concentration, BC concentration, or BrC absorption at 365 nm versus CO concentrations to determine
249 the respective NEMRs).

2.4.2. Determining Smoke Sources and Plume Age

251 To match specific fires to observed smoke at the monitoring sites, several methods were used. Data from the
252 Fire Information for Resource Management System (FIRMS) provided active fire data based on thermal anomalies.
253 These are based on measurements from the Moderate Resolution Imaging Spectroradiometer (MODIS), carried by
254 Aqua and Terra satellites, and the Visible Infrared Imaging Radiometer Suite (VIIRS), carried by the Suomi National
255 Polar-orbiting Partnership (Suomi NPP) and NOAA-20 satellites. FIRMS provides live and historical fire maps and
256 data that can be accessed online (https://firms.modaps.eosdis.nasa.gov/). This platform can be used to pinpoint specific
257 locations and obtain distances between points, which is useful for identifying possible fires where smoke was
258 transported to the sampling site and the time for smoke transport when combined with wind speed and direction data.
259 Although the FIRMS fire map is updated every 5 minutes, the polar orbiting satellites pass over the location only
260 twice per day meaning that some fires starting and ending between satellite observations are not detected (Schroeder
261 and Giglio, 2018; Giglio et al., 2021). Also, small or relatively cool fires may not be detected, especially when there
262 is significant cloud coverage, thick smoke, or a continuous, thick forest canopy, which can block satellite detection of
263 prescribed understory burns in forests. Cloud coverage data are available online
264 (https://worldview.earthdata.nasa.gov) and satellite data, including MODIS/VIIRS overpass times, the number of
265 active fire detections per pass, and FRP for all fires that impacted the monitoring sites, can be downloaded from the
266 abovementioned FIRMS website. Burn data provided by Fort Moore were used with the FIRMS data to minimize
267 limitations with each method for identifying sources of observed smoke. For each of the 64 smoke events studied in
268 the paper, burn data are added to the supplementary material (Table S1). Additionally, temperature, relative humidity,
269 and fuel moisture data used can be accessed online through RAWS USA Climate Archive
270 (https://raws.dri.edu/index.html) at the closest to all sites weather station named Ft. Benning, Georgia.
271 The Hybrid Single-Particle Lagrangian Integrated Trajectory (HYSPLIT) model (Stein et al., 2015) was used
272 to calculate back trajectories from monitoring sites. This trajectory analysis was based on meteorological data derived
273 from the Weather Research and Forecasting (WRF) model (Shamarock et al., 2019) enhanced with grid nudging and
274 observational nudging (Deng et al., 2009; Liu et al., 2005), using a 20-minute timestep. The WRF domain settings are
275 shown in Fig. S2. The winds used in the trajectory analysis are from the 1-km grid resolution domain. Each analysis
276 covered a total of 10 trajectories, all below the planetary boundary layer (PBL). HYSPLIT was run with 10-minute
277 timesteps, and the locations of fires were determined based on FIRMS data and the Fort Moore Fire Management
278 records.

3. Results and discussion

3.1. Assessment of PM$_{2.5}$ monitors and background concentrations

The focus of this analysis is on PM$_{2.5}$ mass concentrations from the prescribed fires. Aerosol particle mass concentrations measurements are difficult, especially at background conditions when concentrations are low. Calibrating instruments with known mass standards is also problematic. We performed intercomparisons between monitors including direct comparisons for two pairs (side-by-side) and intercomparison of background PM$_{2.5}$ mass concentrations measured by the study TEOMs to the values reported at state monitoring sites. For example, two TEOMs (used in main and T1293 trailers) collocated at Eglin Air Force Base in 2023 from March 19, 2023 at 8:00 till March 20, 2023 at 10:00, had an orthogonal regression slope of 0.98 ± 0.09, intercept of 0.45 ± 0.37 µg m^{-3} and r^2 of 0.84 (see Fig. S3). The main trailer TEOM was also compared with the TEOM used on T1291 when they were collocated at the Georgia Institute of Technology from September 22, 2023 at 19:00 till October 07, 2023 at 14:00. Although measurement during that period was close to background levels, the comparison resulted in an orthogonal regression slope of 0.88 ± 0.03, intercept of 3.75 ± 0.09 µg m^{-3} and an r^2 of 0.76 (see Fig. S4). The frequency distribution used to determine the mean values, and mean background values of the data recorded at the main trailer and the EPD sites in 2022 are shown in Fig. S5. The mean concentrations in 2022 were 7.02, 9.47, 9.01, 9.26, and 7.11 µg m^{-3} at the main trailer, T1293, T1292, T1921, and T1290 respectively and 10.33 and 10.67 µg m^{-3} at the Columbus Airport and PCSG school EPD sites respectively. Background air PM$_{2.5}$ mass concentrations were also determined by excluding smoke events (discussed below). The monthly backgrounds of PM$_{2.5}$ mass concentrations are shown in Table S2. Background concentrations were in the range of approximately 3–7 µg m^{-3} for monitors at the Fort, and between 7 and 9 µg m^{-3} at the state monitoring sites (Table S3). Higher background PM$_{2.5}$ mass concentrations at the state sites are likely due to the local anthropogenic (urban) influence. These comparisons provide confidence in the mass measurements that cannot be calibrated in a manner similar to gas monitors.

Background concentrations of CO and BC are also given in Table S2. Background CO ranged between ~ 150 and 200 ppb and background BC ranged between 0.14 and 0.57 µg m^{-3}. In terms of spatial variation within Fort Moore, background levels of measured species were slightly lower in sites located far from the main roads and training areas, such as measurements at the main trailer during May of 2021 and the entire 2022 season. No significant temporal variation is observed, although fires within and in the vicinity of the base increase during the transition from winter to spring, indicating that smoke was efficiently dispersed on time scales of approximately one day. Frequent smoke events where concentrations of the various measured species were substantially above these background levels were observed during the 2021 and 2022 field deployments.

3.2. Study of fires at Fort Moore during 2021 and 2022

3.2.1. Overview of the Smoke Detected

We first present an overview of the measurements at Fort Moore during two burning seasons. In the 2021 season, only one research (main) trailer was deployed. In the following year, four more were deployed for a total of five sites.

314   On March 18, 2021, a fully equipped trailer was deployed in the Northern boundary of Fort Moore, and we
315   sampled at that location until April 26, 2021. It was then moved to the center of the Fort for sampling from April 26
316   to May 15, 2021 (see Fig. 1a). During this period, peaks of measured species were observed, as shown in the time
317   series of $PM_{2.5}$ mass in Fig. 2b. A peak of a measured species is defined as the highest value observed within the data
318   points, spanning from an initial rise until a return to background levels. Maximum $PM_{2.5}$ mass concentrations reached
319   2000 μg m^{-3} for 20-minute averaged data and 1400 μg m^{-3} for hourly-averaged data (Table S4). A total of 11 $PM_{2.5}$
320   peaks with mass concentrations greater than 35 μg m^{-3} were recorded. In 2022, over the course of the entire burning
321   season, 32 days recorded a total of 53 $PM_{2.5}$ mass concentration peaks greater than 35 μg m^{-3} across the five measuring
322   sites, as shown in Fig. 2c with similar high concentrations, reaching 841 μg m^{-3} for 20-minute averaged and 513 μg
323   m^{-3} for hourly-averaged data (Tables S5 to S8).

324   We focus on smoke plumes with higher $PM_{2.5}$ mass concentrations to identify their sources and estimate the
325   emissions and evolution of $PM_{2.5}$ mass because the burning areas are readily identified (e.g., detected remotely by
326   satellite) and the plume can be easily delineated from the background. An increase in measured species is considered
327   a peak, or event, when the 20-minute average $PM_{2.5}$ mass is greater than 35 μg m^{-3} and the 40-minute average $PM_{2.5}$
328   mass concentration (average of two consecutive measurements) is larger than 30 μg m^{-3}. This excludes shorter
329   transient events that includes a passing vehicle that can occur at measuring sites near training areas.

330   The large peaks in $PM_{2.5}$ mass are always accompanied by an increase in CO, BC, and BrC. Figure 3 shows
331   the scatter plots of 20-minute averaged data collected in 2021 and 2022. The linear relation between $PM_{2.5}$ and CO,
332   BC, and BrC during events resulted in an r^2 of 0.85, 0.68, and 0.71 respectively. On the other hand, for non-events
333   data, which include all observations during the entirety of the measurement period, r^2 drops to 0.12, 0.33, and 0.17 for
334    $PM_{2.5}$ mass vs CO, BC, and BrC respectively. These correlations suggest that the events identified correspond to
335   periods of measuring smoke from biomass burning sources. However, it is important to note that variability still exists
336   in slopes among different events, which will be explored and discussed in later sections.

337   **3.3. Determining smoke sources**

338   To study the emission and evolution of smoke plumes and make our measurements useful for evaluating
339   smoke transport and dispersion models, we aim to link identified smoke plumes to specific burn areas and determine
340   their transport time. Attribution of the smoke to specific fires is also useful for assessing the impacts of a specific
341   prescribed burning program, such as the one at Fort Moore. Identifying the location of prescribed fires was
342   complicated by several factors. In this study, we had limited beforehand information on the timing and location of
343   planned burns from the burn managers. Moreover, smoke from other sources, such as prescribed and wildfires in the
344   region, but not within the Fort, as well as uncertainty and variability in wind patterns at the time of burning, led us to
345   utilize multiple methods to determine the source of each identified smoke episode.

346   Our analysis started by using satellite data from FIRMS to identify locations of fires (when the satellite passed
347   overhead). After the end of the study, those locations were verified by cross-referencing with the Fort Moore fire
348   management reports, which provided locations and acreage of prescribed burns and ongoing wildfires exclusively
349   within the Fort for each day. Afterwards, we pinpointed the source of smoke that reached the monitors by averaging

11

350   the wind vectors at and before the peaks using the meteorological data from RAWS. This provided the expected

351   general upwind region the smoke likely came from. We also used the HYSPLIT model to conduct back trajectory

352   analysis from the measurement trailer for 8 hours prior to ascertain if the airmass containing the measured smoke had

353   passed the satellite-identified hot spot or the units reported as burnt by the Fort's Fire Management. HYSPLIT initial

354   altitudes were determined by the PBL height, where trajectories for 10 equally distributed altitudes between 10 m

355   above the surface and the top of the PBL were generated for each simulation. For example, if the PBL height was 100

356   m, trajectories were calculated at 10, 20, 30, 40, 50, 60, 70, 80, 90, and 100 m.

357   Through the systematic combination of these methods, we attempted to identify specific fire sources

358   associated with each observed smoke event and the time of transport of the smoke from the fire to the measurement

359   site (referred to as smoke age). This procedure was successful for 61 out of 64 of the identified smoke events. We

360   failed to identify 3 events that had no apparent source in agreement with the studied wind patterns. Moreover, of the

361   61 identified smoke events, 7 events were matched to different sources using the observed wind vector method versus

362   using the HYSPLIT trajectories, 7 events were matched to sources using HYSPLIT only, and 5 events were matched

363   to sources using wind vector method only.

364   The variability of smoke sources determined in some cases is attributed to the difference between wind

365   direction used by HYSPLIT and that recorded by RAWS used for the wind vector calculation. In HYSPLIT, wind

366   data are derived from the three-dimensional wind fields predicted by the application of the WRF model. Figure 4

367   shows a comparison between modeled and observed wind direction during the events identified in 2021 and 2022 at

368   the main trailer. A closer alignment in wind direction is observed during higher-speed wind conditions.

369   As an example of source determination, Figure 5a shows the time series of CO, $PM_{2.5}$ mass, BC, and BrC

370   during three smoke episodes recorded on April 6, 7, and 8, 2021, which are indicated by blue, yellow, and green

371   shading, respectively. Along the top of the graph are the hourly averaged wind vectors based on data from RAWS.

372   Note the high correlation between $PM_{2.5}$ mass and CO concentration and BrC absorption coefficient indicating that

373   the $PM_{2.5}$ peaks were due to smoke. During those three days, the three events were measured during late evening,

374   nighttime, and early morning periods. In each case, there is a time delay between when the burning occurred and when

375   the plume was measured, due to the transport time. In all three cases, burning regions at the Fort were identified as

376   the source. Consider the first smoke event detected at the trailer between 1:00 and 11:00 on April 6, 2021 (blue shaded

377   region in Fig. 5a). Figure 5b shows the map of the Fort and FIRMS satellite data on the day before (April 5, 2021)

378   indicating 2 hot spots on the base, which were later verified in the fire report as burning of 2 units and 4 sections of a

379   third unit. Both burns were to the south and south-southeast of the trailer, and the winds were from the westerly during

380   the daytime on April 5, 2021. By midnight, the wind direction shifted, with air flowing from the south and the

381   southeast, transporting smoke to the trailer's location, leading to elevated concentrations of species on monitors. Wind

382   speeds were very low at night. At about 8:00, wind speed increased, its direction changed, and concentrations of the

383   species all dropped.

384   Burning of other units took place on April 6, 2021 at distances 0.8, 2.1, 2.5, 6.3, and 7.2 miles from the trailer.

385   The level of measured smoke products started increasing in the evening after the winds became southwesterly and

386   stayed high until the morning of the next day (April 7, 2021) (yellow shaded region in Fig. 5a). Later at night of April

387   7 (green shaded region in Fig. 5a), concentration levels increased slightly after the burning of two connected units to

388   the south of the base during the daytime of April 7, 2021 at a distance ranging between 10.8 and 12.5 miles as indicated

389   by the Fort's Fire Management and seen on FIRMS. HYSPLIT back trajectory analysis, shown in Fig. 5 (e, f, and g),

390   was conducted for assessing our conclusion on the sources, especially in cases of wind variation and/or multiple fires

391   such as for the peaks monitored on April 6 (blue shaded region in Fig. 5a) and April 7, 2021 (yellow shaded region in

392   Fig. 5a). Since there are multiple fires on the Fort all in the same southern direction relative to the trailer, the exact

393   source cannot be determined solely based on wind vectors from RAWS data. In these cases, HYSPLIT back

394   trajectories help to pinpoint the exact fire or fires contributing to the smoke event observed. In both cases on April 6

395   (blue shaded region in Fig. 5a) and April 7, 2021 (yellow shaded region in Fig. 5a), the closer fire was the source of

396   smoke as shown in Fig. 5e and 5f.

3.4. Determining smoke age

398   An estimate of the smoke age is needed to separate fresh from aged smoke to estimate emissions of various

399   species (i.e., in fresh smoke) and the changes in their concentrations with plume age. The physical age of smoke is the

400   time it takes the smoke to be transported from the source to the monitoring sites. Following the concept presented for

401   source identification, the transport time of smoke is estimated by averaging wind speed over the period it takes for the

402   smoke to travel from the fire to the measurement sites, determined by iteration (mean wind speed recalculated with

403   new transport time, until convergence). When the average wind speed in the hour leading up to the peak does not

404   result in a smoke age of one hour or less, we begin iterative steps by calculating the average wind vector for additional

405   one hour increments at a time. A detailed example on using average wind vector in estimating the physical age of

406   smoke is provided in the Supplemental section S.1. It is important to note the uncertainty in the estimated smoke age

407   using this method for smoke monitored before and after the peak (maximum concentration), particularly when the

408   smoke event duration (from the start to the end of smoke monitoring) is prolonged, and when wind conditions are

409   highly variable. The age was also determined from the HYSPLIT back trajectories as the time when the lowest

410   trajectory intersects the source of smoke identified. The backward trajectory is initiated from the start time of the

411   smoke event. Due to uncertainties in the WRF simulated winds, particularly at night when wind speeds are low, the

412   backward trajectory occasionally missed the source. Therefore, a series of HYSPLIT simulations with 20-minute

413   intervals from the event start time until the source of smoke could be identified were conducted. The 20-minute interval

414   was chosen based on the temporal resolution of the WRF data.

415   For the three events discussed in Fig. 5, physical ages estimated using the wind vector averaged from

416   observed RAWS wind data are 75 minutes for April 6 (blue shading), 14 minutes for April 7 (yellow shading) and

417   162 minutes for April 8 (green shading), 2021 events. For the same events and using HYSPLIT trajectories closest to

418   the surface and passing through the identified sources, ages were estimated as 130 minutes for April 6 (blue shading),

419   10 minutes for April 7 (yellow shading), and 40 minutes for April 8 (green shading). Based on our analysis, April 6

420   (blue shading) stands out as the only case where the HYSPLIT age exceeds that estimated using the mean wind vector

421   for the same fire source. The difference between modeled and observed wind for these three instances was further

422   investigated by comparison with the observed wind at Columbus Airport. As shown in Fig. S6, the wind direction

423   observed at the airport aligns more closely with that observed at the RAWS site in Fort Moore (though with faster

424   winds at the airport, likely due to the forest canopy effect on wind flow) than with the WRF modeled winds at both

425   sites. However, it is difficult to determine which method is more reliable for studying any specific smoke event. For

426   all the smoke plumes identified, the age of smoke estimated based on HYSPLIT back trajectories ranged from 10

427   minutes (single timestep of trajectory) to 6 hours (36 timesteps), and from a few minutes to 8 hours based on average

428   wind vector method (Table S10). A comparison summary between wind speeds observed by the RAWS and those

429   modeled by WRF during all the events identified in 2021 and 2022 at the main trailer is shown in Fig. 6a. The observed

430   weak correlation ($r^2 = 0.29$) could be due to several factors. For the wind vector analysis, observed winds are measured

431   at one location and 2 meters above ground level with a single monitor, which may not accurately represent the wind

432   patterns along the entire smoke transport path, especially in forested areas where the canopy can affect the wind flow

433   (Mallia et al., 2020). On the other hand, WRF simulates winds for 34 layers at different altitudes from 10 m, being the

434   lowest, to levels higher than the PBL. HYSPLIT applies bilinear interpolation to the data from WRF for the 10

435   trajectories that it calculates, introducing additional uncertainty to the wind patterns used in the simulations. Although

436   the comparison between ages estimated based on the two different methods resulted in reasonable correlation ($r^2 =$

437   0.59), the slope clearly indicates a significantly higher estimation of age when using the wind vector method,

438   particularly for more aged smoke events, as shown in Fig. 6b, where ages from the two methods show stronger

439   agreement for fresh smoke. This can be attributed, in many cases, to the uncertainty in observed winds during low-

440   speed wind conditions, the measurement being far from where winds are observed (RAWS), and most importantly

441   that RAWS measures winds at 2 m above ground level whereas smoke transport happens at higher altitudes with

442   stronger winds. There are additional discrepancies resulting from wind variation at each altitude at which HYSPLIT

443   is running.

3.5. Limitations of the fixed site method

445   The goal of this project is to study the emissions and evolution of smoke from prescribed fires and provide

446   data to test model simulations and assessments of prescribed burning impacts. Some limitations and challenges are

447   associated with our approach of collecting data from a network of fixed sites.

3.5.1. Identification of burning regions

449   First, due to the limitations of satellite fire detection, some fires were not seen in FIRMS satellite detection

450   data but were subsequently identified from the fire management report, such as the prescribed fires on March 23,

451   2021, shown in Fig. S7a. The 20-minute averaged $PM_{2.5}$ mass concentration at the trailer increased to 74.8 µg m^{-3}, and

452   to 47.8 µg m^{-3} hourly average at the EPD site located off-base at the Columbus Airport in the afternoon of March 23,

453   2021, as shown in the time series of Fig. S7b. This increase was accompanied by an elevation in the levels of CO,

454    $PM_{2.5}$ mass, BC, and BrC measured at the trailer. This is an example of burning on the Fort likely affecting the nearby

455   urban population. Prevailing winds were from the southeast at the time of the smoke event, as can be seen from the

456   wind vectors presented on the same time series in Fig. S7b. However, FIRMS satellite data showed no hotspots on the

457   Fort during the entire day. After checking the fire management report for 2021, prescribed burns for 3 units located in

458 the east central part of the Fort at distances ranging from 8.1 to 14.7 miles from the trailer were identified. Looking at

459 either the wind vector at the time of the peak or the HYSPLIT back trajectories, the source of the smoke event

460 identified on March 23, 2021 matches the closer prescribed burn conducted on the Fort.

461   Another issue with this approach is that relying only on data from the burning authorities at Fort Moore can,

462 in some cases, be insufficient due to the lack of information about fires taking place off-base by landowners, such as

463 the off-base fire seen on FIRMS during three overpasses of satellites at 12:38, 13:54, and 14:42 (Fig. S8a). On May

464 9, 2022 at 16:30, monitored species increased at the main trailer and 20 minutes average of $PM_{2.5}$ mass reached 52.3

465 $\mu g\ m^{-3}$ (Fig. S8b). The Fort's Fire Management reported no prescribed fires and one wildfire in the southern part of

466 the base with an indication of zero probability of smoke from that fire reaching the trailer based on wind patterns.

467 Based on both wind vectors and HYSPLIT simulations, the source of the event was identified as an off-base fire

468 detected to the northeast of Fort Moore. The same smoke event was also observed at multiple trailers operating at the

469 time and will be discussed more in the following section.

470 **3.5.2. Identifying a specific fire impacting the site when multiple burning is occurring**

471   When multiple fires are taking place simultaneously in varying wind conditions it can be difficult identifying

472 the specific fire impacting the site, which can lead to uncertainty in the smoke age. This occurred in smoke detected

473 around midnight on March 14, 2022 (see Fig. S9a). Relying on wind data, the smoke source is likely one or more of

474 the fires on the east and/or southeast side of the base with a zero probability of it being one of the fires in the northern

475 part of the base. HYSPLIT may help in narrowing down the possibilities of the smoke source (Fig. S9b), but there is

476 still uncertainty in linking the specific fire to the observed event.

477   When several burning units are in close proximity and near the measurement site, identifying the specific

478 source and smoke age can also be difficult (for example see Fig. S10). In this case burning in three units indicated by

479 the Fort's Fire Management occurred at the same time close to each other and the trailer (distances of 0.6, 1.4, and 2.2

480 miles from the trailer). HYSPLIT trajectory at lowest altitude passes near (to the east), but not over the prescribed

481 fires. Wind direction at the time of the event suggests influence of a minor portion from the northern part of the fire.

482 It is important to note that in such cases, transport near the surface may be heavily influenced by fire-atmosphere

483 interactions, making it difficult to rely on data from RAWS or WRF simulations as accurate indicators of atmospheric

484 flows close to an active fire.

485   We note that there is no direct correlation between the amount of smoke reaching the trailer, i.e., measured

486 species concentrations, and the distance of the fire from the monitoring site. The relation depends on the smoke

487 transport and dispersion that may allow smoke to either directly hit the measuring site, partially reach the measuring

488 site, or pass above the trailer with little or no smoke detection by the monitors. To illustrate this, we compare three

489 case studies. Looking again at the smoke event of February 11, 2022 shown in Fig. S10, smoke reaching the trailer

490 from 0.6 to 2.2 miles fires resulted in a 20-minute maximum $PM_{2.5}$ mass of 62.8 $\mu g\ m^{-3}$ and CO concentration of 1.3

491 ppm at 13:30. On February 12, 2022 (Fig. S11 a and b), smoke from burns of units at distances 4.3 to 4.6 miles from

492 the trailer, caused an increase in 20-minute $PM_{2.5}$ mass concentration to 60 $\mu g\ m^{-3}$ and CO to 0.9 ppm at 13:50, whereas

493 on the night of April 4, 2022 until the morning of April 5, 2022 (Fig. S11 c and d), smoke from fires 3.8 and 3.9 miles

494 from the trailer, caused an increase of 20-minute $PM_{2.5}$ mass concentration to 319 µg m^{-3} and CO to 3.0 ppm at 1:10

495 over a longer smoke monitoring period. The much higher $PM_{2.5}$ mass concentrations measured on April 4, 2022

496 suggests that the trailer received a more direct smoke hit on that day than on February 11, 2022 or February 12, 2022,

497 despite the fire being closer on February 11 and having a very similar distance to the one detected on February 12.

498 This can also be attributed to the much lower nighttime PBL on April 4, which was 9.8 m and caused all HYSPLIT

499 trajectories to overlap as shown in Fig. 12d. Emissions from a smoldering fire with very little buoyant energy were

500 most likely trapped in this shallow layer leading to high concentration measurements. During the daytime on February

501 11 and 12, higher PBL of 1645 and 1305 m, respectively, favored more vertical dispersion of smoke.

3.5.3. Smoke not detected although regions of burning identified

503   On certain days, based on the wind data and the information presented in the fire management report, it

504 appears likely that smoke from the fires at the base should reach specific monitoring sites. However, during those

505 instances, such as the situation on February 15, 2022 shown in Fig. 7, no significant smoke peaks were detected. To

506 explain this outcome, two HYSPLIT forward trajectory simulations were run. The simulations show that if the fire

507 starts at 10:00, the smoke will not intercept the monitor, but if it starts at 11:00, the smoke at higher altitudes has a

508 slight chance of reaching the monitor. Overall, regardless of wind direction favoring smoke transport to monitors,

509 other factors like dispersion and smoke plume behavior, such as lofting, play a significant role in the transport process.

3.6. Using multiple monitoring sites to increase chances of measuring smoke and studying smoke evolution

511   There are distinct advantages of setting up multiple measuring sites and studying smoke over an extended

512 period. First, it helps capture more smoke events, as seen during the 2022 study in comparison with that in 2021 when

513 a single trailer was used. It minimizes issues with predicting downwind locations and is not affected by uncertainty in

514 planned burning locations and times. Second, it reduces the labor and time required for relocating a single trailer and

515 setting it up several times throughout a prescribed burning period where burning occurs over different regions. Third,

516 it provides high spatial resolution and occasionally smoke from the same fire is detected at several sites, which can be

517 useful in studying smoke chemical evolution with higher certainty than studies of multiple plumes of varying ages

518 measured on different days.

519   An example of the same fire detected at several sites is shown in Fig. 8. On May 9, 2022, each of T1291,

520 T1292, Main Trailer, and T1293 detected an off-base fire taking place approximately 11 miles to the north northeast

521 of the base, as shown in Fig. 8a. T1291, the closest trailer to the fire, measured $PM_{2.5}$ mass and CO peaks at 15:10.

522 The time series of species measured in the various trailers is shown in Fig. 8. Subsequent peaks in $PM_{2.5}$ mass, CO,

523 BC, and O_3 concentrations were recorded at T1292, at 15:50, then at the main trailer at 16:30, and finally at T1293,

524 the furthest trailer from the fire, at 18:10 local time. For O_3, note the O_3 enhancement (ΔO_3) superimposed on the

525 diurnal O_3 trend. The ages of the smoke detected based on wind vector analysis were 266, 296, 330 and 480 minutes,

526 for the various trailers. The difference in smoke age is close to the difference in peak arrival times with maximum

527 $PM_{2.5}$ mass concentration observed at 15:02, 15:53, 16:25, and 18:16 on T1291, T1292, T1293, and T Main,

528 respectively. The differences in peak concentrations can be due to a number of factors, including changes in fire

529　emissions with time, extent of plume dilution with distance from the fire and changes in what portions of the plume

530　were measured due to changes in winds. Wind vectors are shown at the top of plots in Fig. 8. Wind direction and

531　speed varied during the period when the plumes were recorded; wind direction was between 52° and 86° from 11:00

532　till 14:00 and speeds between 3 and 7 mph on May 9, 2022. A shift in wind direction to 348° at a speed of 4 mph

533　happened at 15:00. Then, the wind direction fluctuated between 11° and 44°, before wind speed decreased to 0 mph

534　at 20:00 and remained calm until the morning of May 10, 2022. Normalizing these plume data by a stable smoke

535　tracer, such as CO, can account for some of these factors when comparing emissions and evolution of various plume

536　properties.

3.7. Interpretation of measurements to characterize smoke emissions and evolution

3.7.1. $PM_{2.5}$ emissions

539　　　We used the normalized excess mixing ratio (NEMR) to study the emissions of $PM_{2.5}$ species and their

540　evolution in the various measured smoke plumes. The NEMRs determined from the linear regression slopes of $PM_{2.5}$

541　species (mass concentration, BC concentration, BrC absorption versus CO, with backgrounds subtracted) and

542　correlation values (r^2) for all smoke events are summarized in Table 1. $PM_{2.5}$ mass concentration NEMRs from other

543　studies are summarized in Table S11.

544　　　The NEMR of fresh smoke near a fire is interpreted as an emission ratio (ER), assuming the smoke has

545　undergone limited chemical and/or physical changes. ERs based on NEMRs are widely used (Liu et al., 2017b; Collier

546　et al., 2016; Burling et al., 2011; Gkatzelis et al., 2024). They are compiled in reviews and emission inventories for

547　ambient (Andreae, 2019; Prichard et al., 2020) and laboratory fire studies (Yokelson et al., 2013), and for evaluating

548　or making model predictions (Xiu et al., 2022; Jaffe et al., 2022).

549　　　By focusing on fresh smoke (age less than 1 hour), the emissions ratios (ER) of the prescribed fires can be

550　estimated and compared to those from other studies. The $PM_{2.5}$ mass concentration ER ranged between 0.04 and 0.18

551　µg m^{-3} ppb^{-1} and is shown in Fig. 9. These ERs are comparable to other prescribed fires measured at both ground level

552　(Alves et al., 2010; Desservettaz et al., 2017; Korontzi et al., 2003; Balachandran et al., 2013) and aloft in airborne

553　studies (Sinha et al., 2003; May et al., 2014; Gkatzelis et al., 2024; Travis et al., 2023) that span a large range of

554　burning conditions and fuels (details are provided in Table S11). The mean $PM_{2.5}$ mass concentration ER for our data

555　is 0.117 ± 0.045 µg m^{-3} ppb^{-1} and that of these other prescribed fire studies are 0.098 ± 0.034 µg m^{-3} ppb^{-1} for ground-

556　based and 0.188 ± 0.154 µg m^{-3} ppb^{-1} for airborne measurements. There is substantial and similar variability in the

557　ground-based measurements of prescribed fire ERs in this study relative to other studies. More recent airborne-

558　measured prescribed fires have reported substantially higher ERs (Fig. 9). Smoke transported for 10 minutes from the

559　Blackwater river state forest prescribed fire reported by Gkatzelis et al. had an ER of 0.462 µg m^{-3} ppb^{-1} (Gkatzelis et

560　al., 2024) and Travis et al. reported a range of 0.188-0.433 µg m^{-3} ppb^{-1} for 22 prescribed fires studied and grouped

561　into 4 categories based on fuel type (Travis et al., 2023). Figure 9 also shows comparisons with wildfires reported in

562　other studies (Liu et al., 2017b; Collier et al., 2016; Palm et al., 2020; Gkatzelis et al., 2024). Wildfire $PM_{2.5}$ mass ERs

563　are significantly higher than ERs for prescribed fires in this work, with ER ranges between 0.04 and 0.43 µg m^{-3} ppb^{-}

564　^{1} and a mean of 0.264 ± 0.091 µg m^{-3} ppb^{-1} for wildfires, and the difference is statistically significant (two-tailed p

565 value is < 0.0001). Lower $PM_{2.5}$ mass ERs from smaller prescribed fires has been noted in other studies (Liu et al.,

566 2017b) and supports utilizing prescribed burning as a land management tool to limit wildfires. However, differences

567 in altitude at which the measurements were made may have some effect on ERs. Selimovic et al. (Selimovic et al.,

568 2019) noted that the $PM_{2.5}$/CO in ground-level smoke was about half of that observed from aloft apparently due to

569 reduction in aerosol mass from evaporation of semi-volatile aerosol particle components resulting from higher surface

570 temperatures compared to aloft. Pagonis et al. also found airborne OA NEMRs to be a factor of 2 higher than ground-

571 based NEMRs giving the same interpretation (Pagonis et al., 2023). When comparing ERs of prescribed fires in ground

572 versus airborne studies of prescribed fires, shown in Fig. 9, the mean of airborne studies is a factor of ~ 1.9 higher

573 than ground-based studies and the difference is statistically significant (p value is 0.025).

574   This analysis assumes no significant changes in $PM_{2.5}$ mass for smoke less than 1 hour old. We have seen

575 that smoke detected in the afternoon can have enhanced O_3 concentrations, which may also lead to secondary aerosol

576 formation. Smoke plumes with enhanced O_3 are identified in the ERs shown in Fig. 9 and indicate no bias within the

577 range of ERs recorded, suggesting possible secondary aerosol formation within the first hour following emissions

578 does not contribute to the ER variability. We also did not find evidence of ERs depending on time of day. No difference

579 was seen between ERs for fires that started on the same day of measurement (i.e., all detected after 9:00 and before

580 17:00), and those detected at night, after 17:00, or early in the morning corresponding to fires that started the day

581 before the measurement, but still were estimated to correspond to smoke less than one hour old.

582   We also determined the ERs for BC and BrC. BC ERs were in the range of 0.008–0.022 µg m^{-3} ppb^{-1} with a

583 mean value of 0.014 ± 0.004 µg m^{-3} ppb^{-1}, which are within the range of NEMRs reported in other studies; 0.006 µg

584 m^{-3} ppb^{-1} for prescribed burns in southern African savanna forests (Sinha et al., 2003), 0.020 µg m^{-3} ppb^{-1} for rBC

585 (refractory BC) for prescribed burns of California chaparral forests (Akagi et al., 2012), 0.022 µg m^{-3} ppb^{-1} for

586 chaparral forests (May et al., 2014), 0.006 µg m^{-3} ppb^{-1} for fires in Montane ecosystems (May et al., 2014), 0.018 for

587 coastal plain ecosystems in South Carolina (May et al., 2014), and 0.004 µg m^{-3} ppb^{-1} for large wildfires over the

588 western US measured during FIREX (Gkatzelis et al., 2024).

589   The BrC ERs of fresh smoke events ranged between 0.151 and 0.689 Mm^{-1} ppb^{-1} with a mean ± standard

590 deviation of 0.442 ± 0.157 Mm^{-1} ppb^{-1}. There is limited published data on BrC ERs and NEMRs from prescribed fires

591 and the measurement techniques of BrC vary between studies. Liu et al. (Liu et al., 2016) reported aircraft

592 measurements of BrC at 365 nm inferred from PSAP absorption coefficients measured at two wavelengths (470 and

593 532 nm) with an ER of 0.223 ± 0.053 Mm^{-1} ppb^{-1} for fresh agricultural fires in the southeastern US, which is lower

594 than our mean, but falls within the range of values we observed. For large wildfires measured over the western US,

595 Zeng et al. (Zeng et al., 2022) found for Photoacoustic Spectroscopy (PAS) measurements of BrC at a wavelength of

596 405 nm, the ER was 0.131 ± 0.001 Mm^{-1} ppbv^{-1} in plumes < 2 hours old. These values are in the range we recorded,

597 but the BrC ERs for the prescribed fires of this study are more variable.

598 **3.7.2. NEMRs of all smoke events and their change with smoke age**

599   Here we assess the overall variability in NEMRs for $PM_{2.5}$ mass concentrations, BC mass concentrations,

600 BrC absorption coefficients, and AAEs from all the smoke events (including ages less than 1 hour) and assess possible

18

trends with smoke plume age. In this analysis, the observed changes with age are a combination of variability in emissions and evolution of the aerosol since it is not a Lagrangian experiment, meaning that we are not continuously tracking a specific air mass containing smoke particles over time. $PM_{2.5}$ mass concentration NEMRs varied between 0.04 and 0.47 µg m^{-3} ppb^{-1} for all reported events with a mean ± standard deviation of 0.155 ± 0.076 µg m^{-3} ppb^{-1} (median is 0.138 µg m^{-3} ppb^{-1}). BC NEMRs ranged between 0.005 and 0.024 µg m^{-3} ppb^{-1} with a mean value of 0.013 ± 0.005 µg m^{-3} ppb^{-1}. BrC NEMRs ($\Delta BrC/\Delta CO$) varied between 0.133 to 1.550 Mm^{-1} ppb^{-1}. (Note that data collected on April 21, 2022 at trailer 1293 is an outlier with exceptionally high ERs for $PM_{2.5}$ mass concentration and BrC absorption coefficient. The ER for BC mass concentration, while elevated, falls within the observed range. This event corresponds to smoke from an identified prescribed fire at the Fort and has a relatively low ΔCO of 66.1 ppb, which is unexpected given the burn's proximity and the wind speed on that day, causing ERs to be significantly higher. The HYSPLIT back trajectory from the measuring site does not intersect with the fire but passes close to it. Although the FRP reported on FIRMS does not differ from that of other fires, and there is no significant difference in vegetation type or fuel moisture, the most likely explanation for this event is that the smoke passing through the measurement site was not a direct hit but from the diluted boundary of the plume, which may have undergone photochemical processing, leading to higher $PM_{2.5}$, BrC, and O_3 NEMRs.). The NEMRs are given in Table 1 for all smoke events data and plotted in Fig. 10 as a function of estimated smoke age determined from the wind vector and HYSPLIT analysis. From these plots we assess if there is any systematic evolution of the $PM_{2.5}$ mass, BC and BrC.

Changes in $PM_{2.5}$ Mass Concentration NEMR with smoke age: From Fig. 10a, $PM_{2.5}$ mass concentration NEMR shows substantial variability at all ages with no significant statistical difference or clear trend, however, NEMR tends to be lower for fresh smoke events (≤ 1 hour old) versus more aged plumes, possibly from secondary aerosol formation. Considering only smoke plumes in which O_3 enhancements were observed (i.e., smoke measured between 12:00 and 18:00), $PM_{2.5}$ mass concentration NEMR consistently increases with physical age ($r^2 = 0.65$), possibly evidence of secondary aerosol formation driven by photochemistry.

A range of results for changes in $PM_{2.5}$ mass concentration NEMRs in wildland fires have been observed in other studies, including systematic increases, little change, or decreases with smoke age. To the best of our knowledge, no ground-based studies have been conducted on the evolution of smoke from prescribed fires, but frequent airborne studies have investigated prescribed and wildland smoke aging because of the ability to spatially characterize a single plume. While studying two prescribed fires in SC, May et al. (May et al., 2015) observed no statistically significant net change in OA NEMRs near the source and downwind for smoke transported for ≤ 1.5 hours. One of the two fires was studied for longer, and results showed downwind OA NEMRs over 2 to 5 hours of transport significantly lower than the NEMRs at the source, suggesting a net loss of emitted OA. For wildfires, Collier et al. (Collier et al., 2016) found increases, little change, and decreases with smoke age in different wildfire plumes measured in Oregon. For the selected large wildfires in the western US in summer, Palm et al. (Palm et al., 2020) reported that the OA NEMR remained almost constant at a value of ~ 0.25 µg m^{-3} ppb^{-1} as the plume aged from 20-50 minutes to 6 hours. In their analysis of the data of wildland fires studied during FIREX-AQ campaign in 2019, Pagonis et al. report OA NEMR increased from 0.2 g g^{-1} to 0.3 g g^{-1} in 3 hours (Pagonis et al., 2023). While Garofalo et al. found no significant change of NEMRs between 0.5-8 hours transport of smoke from 20 western wildfires, they concluded that there was secondary

638   OA formation through oxidation driven condensation, but it was balanced by dilution-driven evaporation (Garofalo et

639   al., 2019). Gkatzelis et al. reported the NEMRs of some plumes that were more than an hour old and are shown in

640   Table S11 with their corresponding physical age (Gkatzelis et al., 2024). For the same fire (William's flat), the NEMR

641   was 0.331 µg m^{-3} ppb^{-1} at a physical age of 15 minutes that increased to 0.524 µg m^{-3} ppb^{-1} at 102 minutes (Gkatzelis

642   et al., 2024). Similar increase for the Castle fire was seen where the NEMRs reported are 0.204, 0.244, and 0.463 µg

643   m^{-3} ppb^{-1} at 25, 27, and 153 minutes respectively. For another fire (Horsefly), the NEMR was 0.398 µg m^{-3} ppb^{-1} at a

644   physical age of 65 minutes and remained at a similar value of 0.391 µg m^{-3} ppb^{-1} at 104 minutes. On average, the mean

645   NEMRs for plumes of physical age less than one hour, reported in their study, was 0.218 ± 0.110. This value is lower

646   than that of plumes older than one hour, which have a mean value of 0.391 ± 0.131 (Gkatzelis et al., 2024). Overall,

647   we find no trends in our data when considering all the smoke plumes detected, but for periods of expected

648   photochemical activity we observe consistent evidence for aerosol formation with plume age, which might be

649   attributed to the optically thin smoke that allows photochemistry throughout the plume compared to large optically

650   thick wildfires that leads to more complex photochemistry within the plume (Decker et al., 2021a).

651   We examined other factors that may contribute to variability of PM$_{2.5}$ mass NEMRs. No significant difference

652   was observed between on-base and off-base sources of smoke. Mean PM$_{2.5}$ mass NEMR of smoke originating from

653   outside the base is 0.208 (range 0.112–0.277 µg m^{-3} ppb^{-1}), compared to 0.147 µg m^{-3} ppb^{-1} (range 0.042– 0.466 µg

654   m^{-3} ppb^{-1}) for on base burning, which is not statistically different (two tailed p-value is 0.076). A preliminary

655   assessment using Google Earth satellite imagery and Landscape Fire and Resources Management Planning Tool

656   (LANDFIRE, https://www.landfire.gov/) does not show any visible differences in vegetation between the forested

657   areas burnt on and off the base. Additionally, no further information regarding the fuel types in the off-base lands

658   could be obtained. Just like no detected differences being observed between day/night PM$_{2.5}$ mass concentration ERs,

659   there was no significant difference (p-value is 0.169) between smoke plumes of all ages measured during the day

660   corresponding to fires occurring within a few hours from starting the burn (after 9:00 and before 17:00) (mean NEMR

661   = 0.178 µg m^{-3} ppb^{-1}) and those monitored at night and early in the morning corresponding to fires starting the day

662   before (after 17:00) (mean NEMR = 0.137 µg m^{-3} ppb^{-1}), in contrast to an observed trend of PM$_{2.5}$ mass NEMR with

663   age for smoke with O$_3$ enhancement. This may suggest little night-time secondary aerosol formation (Brown et al.,

664   2013), but a more focused analysis is needed to better assess possible evidence for secondary aerosol formation. No

665   correlation was observed between PM$_{2.5}$ mass NEMRs and relative humidity (r^2 = 0.08) or fuel moisture data (r^2 =

666   0.04) for the smoke events in this study (Fig. S13). A weak positive correlation between air temperature and PM$_{2.5}$

667   mass NEMRs was observed, with an r^2 of 0.14 for all smoke events and r^2 of 0.44 for fresh smoke events. Many factors

668   could cause variability in PM$_{2.5}$ mass NEMRs, but no single factor could be identified when all data from this study

669   is grouped together.

670   ***Changes in BC and BrC NEMR with smoke age:*** BC and BrC NEMRs versus age are shown in Fig. 10b

671   and 10c with periods of O$_3$ enhancements identified. No trend in BC NEMRs with age is observed, as expected, since

672   BC is primarily emitted and largely nonvolatile. Lack of a trend supports this analysis approach, and all the BC

673   measured in events largely reflects BC variability in emissions relative to CO. BrC NEMRs are also highly variable

674   and have no trend with age for all the data or just the periods of O$_3$ enhancements. Since BrC can be both primary and

secondary, is semi-volatile, and undergoes photo-bleaching, a range of results on BrC evolution has been observed in past studies (Zhong and Jang, 2014; Saleh et al., 2013; Liu et al., 2016). Like BC, a similar large variability, with no trend, in BrC NEMRs with ages up to 8 hours has been observed for wildfires in the western US (Zeng et al., 2022; Sullivan et al., 2022; Palm et al., 2020) whereas in some cases consistent loss (bleaching) of BrC has been reported (Forrister et al., 2015). Optical properties of absorptive aerosol spectral properties characterized by AAE are shown in Fig. 11 as a function of age. Total absorption AAE values from the two trailers with 7-wavelength aethalometers (i.e., BC+BrC measured by the aethalometer) varied between 1.31 and 3.32 (mean ± stdev of 1.89 ± 0.23) and between 3.19 and 7.43 (mean = 5.00 ± 0.89) for BrC only. AAEs have no trend with age for either fresh smoke plumes or periods of O_3 enhancement. While our total AAE values are similar (Zeng et al., 2022; Strand et al., 2016; Marsavin et al., 2023) or sometimes lower (Liu et al., 2016; Forrister et al., 2015) than those in other biomass burning studies, it is indicative of the presence of BrC in the smoke plumes studied. As for BrC AAEs, our reported values are significantly higher than those reported for western wildfires, where BrC determined from the PAS had an AAE of 2.07 ± 1.01 (Zeng et al., 2022), indicating difference in BrC optical properties or with instrumentation, which needs further investigation. Selimovic et al. show that duff has the highest AAE of 7.13 (calculated from absorption data at 401 and 870 nm) when burnt, and it is typically consumed more in wildfires than in prescribed fires. However, the variability in optical properties is influenced more by the differential consumption of individual components than by the dominant tree species in the ecosystem (Selimovic et al., 2019).

4. Conclusion

We describe a ground-based observational study for characterizing smoke from prescribed fires based on continuous monitoring at multiple sites for an extended period in a regularly burned region. We focus on burning within a large military Fort in the southeastern US and identify the sources of the smoke to determine if it was within or outside the Fort and study emissions and evolution of smoke species. The method was successful in capturing a significant number of smoke events (64) monitored on 42 days and linked to 45 fires across 2 burning seasons. Source and age for each smoke plume detected was estimated. This allowed us to match 95 % of the identified events to their corresponding source and to calculate the estimated transport time of smoke from source to monitors. These data were used to characterize emissions and evolution of key smoke parameters through calculation of normalized excess mixing ratios (NEMRs), with CO as the conserved co-emitted species. Overall, $PM_{2.5}$ mass concentration NEMRs ($\Delta PM_{2.5}$ mass/ΔCO) ranged between 0.04 and 0.47 µg m^{-3} ppb^{-1} with a study mean of 0.155 ± 0.076 µg m^{-3} ppb^{-1} (median is 0.138 µg m^{-3} ppb^{-1}). For plumes less than 1 hour old the $PM_{2.5}$ mass concentration NEMRs were interpreted as a characteristic of the fire's emissions. Emissions ratios for fires of this study ranged between 0.042 and 0.176 µg m^{-3} ppb^{-1} with a mean of 0.117 ± 0.045 µg m^{-3} ppb^{-1} (median is 0.121 µg m^{-3} ppb^{-1}). These emissions estimates are in the range reported in other ground-based studies for a range of fires and fuels but are lower than what has been reported for wildfire smoke measured from aircraft at higher altitudes. BC and BrC NEMRs and emission ratios are also reported. An analysis of $PM_{2.5}$ mass and BrC NEMRs changes with smoke age showed no consistent trends for all combined smoke plumes. However, $PM_{2.5}$ mass NEMRs did increase with age for smoke detected in the afternoon in plumes where O_3 enhancements were observed, indicating the formation of O_3 and secondary aerosol. This was not

21

711 observed for BrC NEMRs. This data set will be used to assess models predicting the impact of prescribed fires on air
712 quality to enhance the use of prescribed burning in land management practices by minimizing impacts on populations.

5. Competing interests

714 The contact author has declared that none of the authors has any competing interests.

6. Acknowledgements

720 **Author contribution:** REA and RJW wrote the paper. RJW, LGH, DJT, and MTO designed the experiment. REA
721 and DJT collected the data. REA, ZL, DJT, and RJW analyzed data. REA and ZL worked on the HYSPLIT analysis.
722 All authors reviewed and provided comments for the paper.

723 **Data availability:** Data are available in a publicly accessible repository: https://doi.org/10.5281/zenodo.11222295.

724   **References**

725   Afrin, S. and Garcia-Menendez, F.: The Influence of Prescribed Fire on Fine Particulate Matter Pollution in the

726   Southeastern United States, Geophys. Res. Lett., 47, https://doi.org/10.1029/2020GL088988, 2020.

727   Akagi, S. K., Craven, J. S., Taylor, J. W., McMeeking, G. R., Yokelson, R. J., Burling, I. R., Urbanski, S. P., Wold,

728   C. E., Seinfeld, J. H., Coe, H., Alvarado, M. J., and Weise, D. R.: Evolution of trace gases and particles emitted by a

729   chaparral fire in California, Atmos. Chem. Phys., 12, 1397–1421, https://doi.org/10.5194/acp-12-1397-2012, 2012.

730   Akagi, S. K., Burling, I. R., Mendoza, A., Johnson, T. J., Cameron, M., Griffith, D. W. T., Paton-Walsh, C., Weise,

731   D. R., Reardon, J., and Yokelson, R. J.: Field measurements of trace gases emitted by prescribed fires in

732   southeastern US pine forests using an open-path FTIR system, Atmos. Chem. Phys., https://doi.org/10.5194/acp-14-

733   199-2014, 2014.

734   Alves, C. A., Gonçalves, C., Pio, C. A., Mirante, F., Caseiro, A., Tarelho, L., Freitas, M. C., and Viegas, D. X.:

735   Smoke emissions from biomass burning in a Mediterranean shrubland, Atmos. Environ., 44, 3024–3033,

736   https://doi.org/10.1016/j.atmosenv.2010.05.010, 2010.

737   Andreae, M. O.: Emission of trace gases and aerosols from biomass burning – an updated assessment, Atmos.

738   Chem. Phys., 19, 8523–8546, https://doi.org/10.5194/acp-19-8523-2019, 2019.

739   Appel, K. W., Bash, J. O., Fahey, K. M., Foley, K. M., Gilliam, R. C., Hogrefe, C., Hutzell, W. T., Kang, D.,

740   Mathur, R., Murphy, B. N., Napelenok, S. L., Nolte, C. G., Pleim, J. E., Pouliot, G. A., Pye, H. O. T., Ran, L.,

741   Roselle, S. J., Sarwar, G., Schwede, D. B., Sidi, F. I., Spero, T. L., and Wong, D. C.: The Community Multiscale Air

742   Quality (CMAQ) model versions 5.3 and 5.3.1: system updates and evaluation, Geosci. Model Dev., 14, 2867–2897,

743   https://doi.org/10.5194/gmd-14-2867-2021, 2021.

744   Aurell, J. and Gullett, B. K.: Effects of UAS Rotor Wash on Air Quality Measurements, Drones, 8, 73,

745   https://doi.org/10.3390/drones8030073, 2024.

746   Aurell, J., Gullett, B., Holder, A., Kiros, F., Mitchell, W., Watts, A., and Ottmar, R.: Wildland fire emission

747   sampling at Fishlake National Forest, Utah using an unmanned aircraft system, Atmos. Environ., 247, 118193,

748   https://doi.org/10.1016/j.atmosenv.2021.118193, 2021.

749   Balachandran, S., Pachon, J. E., Lee, S., Oakes, M. M., Rastogi, N., Shi, W., Tagaris, E., Yan, B., Davis, A., Zhang,

750   X., Weber, R. J., Mulholland, J. A., Bergin, M. H., Zheng, M., and Russell, A. G.: Particulate and gas sampling of

751   prescribed fires in South Georgia, USA, Atmos. Environ., 81, 125–135,

752   https://doi.org/10.1016/j.atmosenv.2013.08.014, 2013.

753   Bell, M. L.: Ozone and Short-term Mortality in 95 US Urban Communities, 1987-2000, JAMA, 292, 2372,

754   https://doi.org/10.1001/jama.292.19.2372, 2004.

755   Bond, T. C., Anderson, T. L., and Campbell, D.: Calibration and Intercomparison of Filter-Based Measurements of

Visible Light Absorption by Aerosols, Aerosol Sci. Technol., https://doi.org/10.1080/027868299304435, 1999.

Borchers-Arriagada, N., Bowman, D. M. J. S., Price, O., Palmer, A. J., Samson, S., Clarke, H., Sepulveda, G., and Johnston, F. H.: Smoke health costs and the calculus for wildfires fuel management: a modelling study, Lancet Planet. Heal., https://doi.org/10.1016/S2542-5196(21)00198-4, 2021.

Brown, S. S., Dubé, W. P., Bahreini, R., Middlebrook, A. M., Brock, C. A., Warneke, C., de Gouw, J. A., Washenfelder, R. A., Atlas, E., Peischl, J., Ryerson, T. B., Holloway, J. S., Schwarz, J. P., Spackman, R., Trainer, M., Parrish, D. D., Fehshenfeld, F. C., and Ravishankara, A. R.: Biogenic VOC oxidation and organic aerosol formation in an urban nocturnal boundary layer: aircraft vertical profiles in Houston, TX, Atmos. Chem. Phys., 13, 11317–11337, https://doi.org/10.5194/acp-13-11317-2013, 2013.

Burling, I. R., Yokelson, R. J., Akagi, S. K., Urbanski, S. P., Wold, C. E., Griffith, D. W. T., Johnson, T. J., Reardon, J., and Weise, D. R.: Airborne and ground-based measurements of the trace gases and particles emitted by prescribed fires in the United States, Atmos. Chem. Phys., 11, 12197–12216, https://doi.org/10.5194/acp-11-12197-2011, 2011.

Christopher, S. A., Chou, J., Welch, R. M., Kliche, D. V., and Connors, V. S.: Satellite investigations of fire, smoke, and Carbon Monoxide during April 1994 MAPS mission: Case studies over tropical Asia, J. Geophys. Res. Atmos., https://doi.org/10.1029/97JD01813, 1998.

Collier, S., Zhou, S., Onasch, T. B., Jaffe, D. A., Kleinman, L., Sedlacek, A. J., Briggs, N. L., Hee, J., Fortner, E., Shilling, J. E., Worsnop, D., Yokelson, R. J., Parworth, C., Ge, X., Xu, J., Butterfield, Z., Chand, D., Dubey, M. K., Pekour, M. S., Springston, S., and Zhang, Q.: Regional Influence of Aerosol Emissions from Wildfires Driven by Combustion Efficiency: Insights from the BBOP Campaign, Environ. Sci. Technol., 50, 8613–8622, https://doi.org/10.1021/acs.est.6b01617, 2016.

Cubison, M. J., Ortega, A. M., Hayes, P. L., Farmer, D. K., Day, D., Lechner, M. J., Brune, W. H., Apel, E., Diskin, G. S., Fisher, J. A., Fuelberg, H. E., Hecobian, A., Knapp, D. J., Mikoviny, T., Riemer, D., Sachse, G. W., Sessions, W., Weber, R. J., Weinheimer, A. J., Wisthaler, A., and Jimenez, J. L.: Effects of aging on organic aerosol from open biomass burning smoke in aircraft and laboratory studies, Atmos. Chem. Phys., https://doi.org/10.5194/acp-11-12049-2011, 2011.

Decker, Z. C. J., Robinson, M. A., Barsanti, K. C., Bourgeois, I., Coggon, M. M., DiGangi, J. P., Diskin, G. S., Flocke, F. M., Franchin, A., Fredrickson, C. D., Gkatzelis, G. I., Hall, S. R., Halliday, H., Holmes, C. D., Huey, L. G., Lee, Y. R., Lindaas, J., Middlebrook, A. M., Montzka, D. D., Moore, R., Neuman, J. A., Nowak, J. B., Palm, B. B., Peischl, J., Piel, F., Rickly, P. S., Rollins, A. W., Ryerson, T. B., Schwantes, R. H., Sekimoto, K., Thornhill, L., Thornton, J. A., Tyndall, G. S., Ullmann, K., Van Rooy, P., Veres, P. R., Warneke, C., Washenfelder, R. A., Weinheimer, A. J., Wiggins, E., Winstead, E., Wisthaler, A., Womack, C., and Brown, S. S.: Nighttime and daytime dark oxidation chemistry in wildfire plumes: an observation and model analysis of FIREX-AQ aircraft data, Atmos. Chem. Phys., 21, 16293–16317, https://doi.org/10.5194/acp-21-16293-2021, 2021a.

790   Decker, Z. C. J., Wang, S., Bourgeois, I., Campuzano Jost, P., Coggon, M. M., DiGangi, J. P., Diskin, G. S., Flocke,

791   F. M., Franchin, A., Fredrickson, C. D., Gkatzelis, G. I., Hall, S. R., Halliday, H., Hayden, K., Holmes, C. D., Huey,

792   L. G., Jimenez, J. L., Lee, Y. R., Lindaas, J., Middlebrook, A. M., Montzka, D. D., Neuman, J. A., Nowak, J. B.,

793   Pagonis, D., Palm, B. B., Peischl, J., Piel, F., Rickly, P. S., Robinson, M. A., Rollins, A. W., Ryerson, T. B.,

794   Sekimoto, K., Thornton, J. A., Tyndall, G. S., Ullmann, K., Veres, P. R., Warneke, C., Washenfelder, R. A.,

795   Weinheimer, A. J., Wisthaler, A., Womack, C., and Brown, S. S.: Novel Analysis to Quantify Plume Crosswind

796   Heterogeneity Applied to Biomass Burning Smoke, Environ. Sci. Technol., https://doi.org/10.1021/acs.est.1c03803,

797   2021b.

798   Deng, A., Stauffer, D., Guadet, B., Dudhia, J., Hacker, J., Bruyere, C., Wu, W., Vandenberghe, F., Liu, Y., and

799   Bourgeois, A.: A. 1.9 Update on WRF-ARW End-to-End Multi-Scale FDDA System, in: In Proceedings of the

800   WRF Users' Workshop, 2009.

801   Desservettaz, M., Paton-Walsh, C., Griffith, D. W. T., Kettlewell, G., Keywood, M. D., Vanderschoot, M. V., Ward,

802   J., Mallet, M. D., Milic, A., Miljevic, B., Ristovski, Z. D., Howard, D., Edwards, G. C., and Atkinson, B.: Emission

803   factors of trace gases and particles from tropical savanna fires in Australia, J. Geophys. Res. Atmos., 122, 6059–

804   6074, https://doi.org/10.1002/2016JD025925, 2017.

805   Fiddler, M. N., Thompson, C., Pokhrel, R. P., Majluf, F., Canagaratna, M., Fortner, E. C., Daube, C., Roscioli, J. R.,

806   Yacovitch, T. I., Herndon, S. C., and Bililign, S.: Emission Factors From Wildfires in the Western US: An

807   Investigation of Burning State, Ground Versus Air, and Diurnal Dependencies During the FIREX-AQ 2019

808   Campaign, J. Geophys. Res. Atmos., 129, https://doi.org/10.1029/2022JD038460, 2024.

809   Fleming, L. T., Lin, P., Roberts, J. M., Selimovic, V., Yokelson, R., Laskin, J., Laskin, A., and Nizkorodov, S. A.:

810   Molecular composition and photochemical lifetimes of brown carbon chromophores in biomass burning organic

811   aerosol, Atmos. Chem. Phys., 20, 1105–1129, https://doi.org/10.5194/acp-20-1105-2020, 2020.

812   Forrister, H., Liu, J., Scheuer, E., Dibb, J., Ziemba, L., Thornhill, K. L., Anderson, B., Diskin, G., Perring, A. E.,

813   Schwarz, J. P., Campuzano-Jost, P., Day, D. A., Palm, B. B., Jimenez, J. L., Nenes, A., and Weber, R. J.: Evolution

814   of brown carbon in wildfire plumes, Geophys. Res. Lett., 42, 4623–4630, https://doi.org/10.1002/2015GL063897,

815   2015.

816   Garcia, A., Santa-Helena, E., De Falco, A., de Paula Ribeiro, J., Gioda, A., and Gioda, C. R.: Toxicological Effects

817   of Fine Particulate Matter (PM2.5): Health Risks and Associated Systemic Injuries—Systematic Review, Water,

818   Air, Soil Pollut., 234, 346, https://doi.org/10.1007/s11270-023-06278-9, 2023.

819   Garofalo, L. A., Pothier, M. A., Levin, E. J. T., Campos, T., Kreidenweis, S. M., and Farmer, D. K.: Emission and

820   Evolution of Submicron Organic Aerosol in Smoke from Wildfires in the Western United States, ACS Earth Sp.

821   Chem., 3, 1237–1247, https://doi.org/10.1021/acsearthspacechem.9b00125, 2019.

822   Giglio, L., Schroeder, W., Hall, J., and Justice, C.: MODIS Collection 6 and Collection 6.1 Active Fire Product

823   User's Guide, Nasa, Version 1., 64, 2021.

Gkatzelis, G. I., Coggon, M. M., Stockwell, C. E., Hornbrook, R. S., Allen, H., Apel, E. C., Bela, M. M., Blake, D. R., Bourgeois, I., Brown, S. S., Campuzano-Jost, P., St. Clair, J. M., Crawford, J. H., Crounse, J. D., Day, D. A., DiGangi, J. P., Diskin, G. S., Fried, A., Gilman, J. B., Guo, H., Hair, J. W., Halliday, H. S., Hanisco, T. F., Hannun, R., Hills, A., Huey, L. G., Jimenez, J. L., Katich, J. M., Lamplugh, A., Lee, Y. R., Liao, J., Lindaas, J., McKeen, S. A., Mikoviny, T., Nault, B. A., Neuman, J. A., Nowak, J. B., Pagonis, D., Peischl, J., Perring, A. E., Piel, F., Rickly, P. S., Robinson, M. A., Rollins, A. W., Ryerson, T. B., Schueneman, M. K., Schwantes, R. H., Schwarz, J. P., Sekimoto, K., Selimovic, V., Shingler, T., Tanner, D. J., Tomsche, L., Vasquez, K. T., Veres, P. R., Washenfelder, R., Weibring, P., Wennberg, P. O., Wisthaler, A., Wolfe, G. M., Womack, C. C., Xu, L., Ball, K., Yokelson, R. J., and Warneke, C.: Parameterizations of US wildfire and prescribed fire emission ratios and emission factors based on FIREX-AQ aircraft measurements, Atmos. Chem. Phys., 24, 929–956, https://doi.org/10.5194/acp-24-929-2024, 2024.

Hecobian, A., Zhang, X., Zheng, M., Frank, N., Edgerton, E. S., and Weber, R. J.: Water-soluble organic aerosol material and the light-absorption characteristics of aqueous extracts measured over the Southeastern United States, Atmos. Chem. Phys., https://doi.org/10.5194/acp-10-5965-2010, 2010.

Huang, R., Hu, Y., Russell, A. G., Mulholland, J. A., and Odman, M. T.: The Impacts of Prescribed Fire on PM2.5 Air Quality and Human Health: Application to Asthma-Related Emergency Room Visits in Georgia, USA, Int. J. Environ. Res. Public Health, 16, 2312, https://doi.org/10.3390/ijerph16132312, 2019.

Ichoku, C. and Kaufman, Y. J.: A method to derive smoke emission rates from MODIS fire radiative energy measurements, in: IEEE Transactions on Geoscience and Remote Sensing, https://doi.org/10.1109/TGRS.2005.857328, 2005.

Jaffe, D. A., O'Neill, S. M., Larkin, N. K., Holder, A. L., Peterson, D. L., Halofsky, J. E., and Rappold, A. G.: Wildfire and prescribed burning impacts on air quality in the United States, https://doi.org/10.1080/10962247.2020.1749731, 2020.

Jaffe, D. A., Schnieder, B., and Inouye, D.: Technical note: Use of PM 2.5 to CO ratio as an indicator of wildfire smoke in urban areas, Atmos. Chem. Phys., 22, 12695–12704, https://doi.org/10.5194/acp-22-12695-2022, 2022.

Jo, D. S., Park, R. J., Lee, S., Kim, S. W., and Zhang, X.: A global simulation of brown carbon: Implications for photochemistry and direct radiative effect, Atmos. Chem. Phys., https://doi.org/10.5194/acp-16-3413-2016, 2016.

Kelp, M. M., Carroll, M. C., Liu, T., Yantosca, R. M., Hockenberry, H. E., and Mickley, L. J.: Prescribed Burns as a Tool to Mitigate Future Wildfire Smoke Exposure: Lessons for States and Rural Environmental Justice Communities, Earth's Futur., 11, https://doi.org/10.1029/2022EF003468, 2023.

Korontzi, S., Ward, D. E., Susott, R. A., Yokelson, R. J., Justice, C. O., Hobbs, P. V., Smithwick, E. A. H., and Hao, W. M.: Seasonal variation and ecosystem dependence of emission factors for selected trace gases and PM 2.5 for southern African savanna fires, J. Geophys. Res. Atmos., 108, https://doi.org/10.1029/2003JD003730, 2003.

857   Kuenzer, C., Hecker, C., Zhang, J., Wessling, S., and Wagner, W.: The potential of multidiurnal MODIS thermal
858   band data for coal fire detection, Int. J. Remote Sens., https://doi.org/10.1080/01431160701352147, 2008.

859   Lack, D. A. and Langridge, J. M.: On the attribution of black and brown carbon light absorption using the Ångström
860   exponent, Atmos. Chem. Phys., 13, 10535–10543, https://doi.org/10.5194/acp-13-10535-2013, 2013.

861   Larkin, N. K., O'Neill, S. M., Solomon, R., Raffuse, S., Strand, T., Sullivan, D. C., Krull, C., Rorig, M., Peterson, J.,
862   and Ferguson, S. A.: The BlueSky smoke modeling framework, Int. J. Wildl. Fire, 18, 906,
863   https://doi.org/10.1071/WF07086, 2009.

864   Larkin, N. K., Raffuse, S. M., Huang, S. M., Pavlovic, N., Lahm, P., and Rao, V.: The Comprehensive Fire
865   Information Reconciled Emissions (CFIRE) inventory: Wildland fire emissions developed for the 2011 and 2014
866   U.S. National Emissions Inventory, J. Air Waste Manag. Assoc., https://doi.org/10.1080/10962247.2020.1802365,
867   2020.

868   Laskin, A., Laskin, J., and Nizkorodov, S. A.: Chemistry of Atmospheric Brown Carbon, Chem. Rev., 115, 4335–
869   4382, https://doi.org/10.1021/cr5006167, 2015.

870   Lee, J. Y., Daube, C., Fortner, E., Ellsworth, N., May, N. W., Tallant, J., Herndon, S., and Pratt, K. A.: Chemical
871   characterization of prescribed burn emissions from a mixed forest in Northern Michigan, Environ. Sci. Atmos., 3,
872   35–48, https://doi.org/10.1039/D2EA00069E, 2023.

873   Lee, S., Baumann, K., Schauer, J. J., Sheesley, R. J., Naeher, L. P., Meinardi, S., Blake, D. R., Edgerton, E. S.,
874   Russell, A. G., and Clements, M.: Gaseous and Particulate Emissions from Prescribed Burning in Georgia, Environ.
875   Sci. Technol., 39, 9049–9056, https://doi.org/10.1021/es051583l, 2005.

876   Lee, S., Kim, H. K., Yan, B., Cobb, C. E., Hennigan, C., Nichols, S., Chamber, M., Edgerton, E. S., Jansen, J. J.,
877   Hu, Y., Zheng, M., Weber, R. J., and Russell, A. G.: Diagnosis of Aged Prescribed Burning Plumes Impacting an
878   Urban Area, Environ. Sci. Technol., 42, 1438–1444, https://doi.org/10.1021/es7023059, 2008.

879   Levy, I., Mihele, C., Lu, G., Narayan, J., Hilker, N., and Brook, J. R.: Elucidating multipollutant exposure across a
880   complex metropolitan area by systematic deployment of a mobile laboratory, Atmos. Chem. Phys.,
881   https://doi.org/10.5194/acp-14-7173-2014, 2014.

882   Li, F., Zhang, X., Kondragunta, S., and Lu, X.: An evaluation of advanced baseline imager fire radiative power
883   based wildfire emissions using carbon monoxide observed by the Tropospheric Monitoring Instrument across the
884   conterminous United States, Environ. Res. Lett., 15, 094049, https://doi.org/10.1088/1748-9326/ab9d3a, 2020.

885   Linn, R. R., Goodrick, S. L., Brambilla, S., Brown, M. J., Middleton, R. S., O'Brien, J. J., and Hiers, J. K.: QUIC-
886   fire: A fast-running simulation tool for prescribed fire planning, Environ. Model. Softw., 125, 104616,
887   https://doi.org/10.1016/j.envsoft.2019.104616, 2020.

888   Liu, D., Zhang, Q., Jiang, J., and Chen, D. R.: Performance calibration of low-cost and portable particular matter

(PM) sensors, J. Aerosol Sci., https://doi.org/10.1016/j.jaerosci.2017.05.011, 2017a.

Liu, J. C., Pereira, G., Uhl, S. A., Bravo, M. A., and Bell, M. L.: A systematic review of the physical health impacts from non-occupational exposure to wildfire smoke, Environ. Res., 136, 120–132, https://doi.org/10.1016/j.envres.2014.10.015, 2015.

Liu, T., Marlier, M. E., Karambelas, A., Jain, M., Singh, S., Singh, M. K., Gautam, R., and Defries, R. S.: Missing emissions from post-monsoon agricultural fires in northwestern India: Regional limitations of modis burned area and active fire products, https://doi.org/10.1088/2515-7620/ab056c, 2019.

Liu, X., Zhang, Y., Huey, L. G., Yokelson, R. J., Wang, Y., Jimenez, J. L., Campuzano-Jost, P., Beyersdorf, A. J., Blake, D. R., Choi, Y., St. Clair, J. M., Crounse, J. D., Day, D. A., Diskin, G. S., Fried, A., Hall, S. R., Hanisco, T. F., King, L. E., Meinardi, S., Mikoviny, T., Palm, B. B., Peischl, J., Perring, A. E., Pollack, I. B., Ryerson, T. B., Sachse, G., Schwarz, J. P., Simpson, I. J., Tanner, D. J., Thornhill, K. L., Ullmann, K., Weber, R. J., Wennberg, P. O., Wisthaler, A., Wolfe, G. M., and Ziemba, L. D.: Agricultural fires in the southeastern U.S. during SEAC4RS: Emissions of trace gases and particles and evolution of ozone, reactive nitrogen, and organic aerosol, J. Geophys. Res. Atmos., 121, 7383–7414, https://doi.org/10.1002/2016JD025040, 2016.

Liu, X., Huey, L. G., Yokelson, R. J., Selimovic, V., Simpson, I. J., Müller, M., Jimenez, J. L., Campuzano-Jost, P., Beyersdorf, A. J., Blake, D. R., Butterfield, Z., Choi, Y., Crounse, J. D., Day, D. A., Diskin, G. S., Dubey, M. K., Fortner, E., Hanisco, T. F., Hu, W., King, L. E., Kleinman, L., Meinardi, S., Mikoviny, T., Onasch, T. B., Palm, B. B., Peischl, J., Pollack, I. B., Ryerson, T. B., Sachse, G. W., Sedlacek, A. J., Shilling, J. E., Springston, S., St. Clair, J. M., Tanner, D. J., Teng, A. P., Wennberg, P. O., Wisthaler, A., and Wolfe, G. M.: Airborne measurements of western U.S. wildfire emissions: Comparison with prescribed burning and air quality implications, J. Geophys. Res. Atmos., 122, 6108–6129, https://doi.org/10.1002/2016JD026315, 2017b.

Liu, Y., Bourgeois, A., Warner, T., Swerdlin, S., and Hacker, J.: Implementation of observation-nudging based FDDA into WRF for supporting ATEC test operations, in: In Proceedings of the WRF/MM5 Users' Workshop, 27–30, 2005.

Mallia, D. V., Kochanski, A. K., Urbanski, S. P., Mandel, J., Farguell, A., and Krueger, S. K.: Incorporating a Canopy Parameterization within a Coupled Fire-Atmosphere Model to Improve a Smoke Simulation for a Prescribed Burn, Atmosphere (Basel)., 11, 832, https://doi.org/10.3390/atmos11080832, 2020.

Mandel, J., Beezley, J. D., and Kochanski, A. K.: Coupled atmosphere-wildland fire modeling with WRF 3.3 and SFIRE 2011, Geosci. Model Dev., 4, 591–610, https://doi.org/10.5194/gmd-4-591-2011, 2011.

Marsavin, A., van Gageldonk, R., Bernays, N., May, N. W., Jaffe, D. A., and Fry, J. L.: Optical properties of biomass burning aerosol during the 2021 Oregon fire season: comparison between wild and prescribed fires, Environ. Sci. Atmos., 3, 608–626, https://doi.org/10.1039/D2EA00118G, 2023.

Martin, M. V., Kahn, R. A., and Tosca, M. G.: A global analysis of wildfire smoke injection heights derived from

space-based multi-angle imaging, Remote Sens., https://doi.org/10.3390/rs10101609, 2018.

Martinsson, B. G., Friberg, J., Sandvik, O. S., and Sporre, M. K.: Five-satellite-sensor study of the rapid decline of wildfire smoke in the stratosphere, Atmos. Chem. Phys., https://doi.org/10.5194/acp-22-3967-2022, 2022.

May, A. A., McMeeking, G. R., Lee, T., Taylor, J. W., Craven, J. S., Burling, I., Sullivan, A. P., Akagi, S., Collett, J. L., Flynn, M., Coe, H., Urbanski, S. P., Seinfeld, J. H., Yokelson, R. J., and Kreidenweis, S. M.: Aerosol emissions from prescribed fires in the United States: A synthesis of laboratory and aircraft measurements, J. Geophys. Res. Atmos., 119, 11,826-11,849, https://doi.org/10.1002/2014JD021848, 2014.

May, A. A., Lee, T., McMeeking, G. R., Akagi, S., Sullivan, A. P., Urbanski, S., Yokelson, R. J., and Kreidenweis, S. M.: Observations and analysis of organic aerosol evolution in some prescribed fire smoke plumes, Atmos. Chem. Phys., 15, 6323–6335, https://doi.org/10.5194/acp-15-6323-2015, 2015.

Mell, W., Jenkins, M. A., Gould, J., and Cheney, P.: A physics-based approach to modelling grassland fires, Int. J. Wildl. Fire, 16, 1, https://doi.org/10.1071/WF06002, 2007.

Melvin, M. A.: 2018 National Prescribed Fire Use Report, 2018.

Melvin, M. A.: 2020 National Prescribed Fire Use Report, 2020.

Melvin, M. A.: 2021 National Prescribed Fire Use Report, 2021.

Mildrexler, D. J., Zhao, M., Heinsch, F. A., and Running, S. W.: A new satellite-based methodology for continental-scale disturbance detection, Ecol. Appl., https://doi.org/10.1890/1051-0761(2007)017[0235:ANSMFC]2.0.CO;2, 2007.

Naeher, L. P., Brauer, M., Lipsett, M., Zelikoff, J. T., Simpson, C. D., Koenig, J. Q., and Smith, K. R.: Woodsmoke Health Effects: A Review, Inhal. Toxicol., 19, 67–106, https://doi.org/10.1080/08958370600985875, 2007.

Nguyen, H. M. and Wooster, M. J.: Advances in the estimation of high Spatio-temporal resolution pan-African top-down biomass burning emissions made using geostationary fire radiative power (FRP) and MAIAC aerosol optical depth (AOD) data, Remote Sens. Environ., 248, 111971, https://doi.org/10.1016/j.rse.2020.111971, 2020.

O'Dell, K., Hornbrook, R. S., Permar, W., Levin, E. J. T., Garofalo, L. A., Apel, E. C., Blake, N. J., Jarnot, A., Pothier, M. A., Farmer, D. K., Hu, L., Campos, T., Ford, B., Pierce, J. R., and Fischer, E. V.: Correction to Hazardous Air Pollutants in Fresh and Aged Western US Wildfire Smoke and Implications for Long-Term Exposure, Environ. Sci. Technol., 56, 3304–3304, https://doi.org/10.1021/acs.est.2c01008, 2022.

Pagonis, D., Selimovic, V., Campuzano-Jost, P., Guo, H., Day, D. A., Schueneman, M. K., Nault, B. A., Coggon, M. M., DiGangi, J. P., Diskin, G. S., Fortner, E. C., Gargulinski, E. M., Gkatzelis, G. I., Hair, J. W., Herndon, S. C., Holmes, C. D., Katich, J. M., Nowak, J. B., Perring, A. E., Saide, P., Shingler, T. J., Soja, A. J., Thapa, L. H., Warneke, C., Wiggins, E. B., Wisthaler, A., Yacovitch, T. I., Yokelson, R. J., and Jimenez, J. L.: Impact of Biomass Burning Organic Aerosol Volatility on Smoke Concentrations Downwind of Fires, Environ. Sci. Technol., 57,

954   17011–17021, https://doi.org/10.1021/acs.est.3c05017, 2023.

955   Palm, B. B., Peng, Q., Fredrickson, C. D., Lee, B. H., Garofalo, L. A., Pothier, M. A., Kreidenweis, S. M., Farmer,
956   D. K., Pokhrel, R. P., Shen, Y., Murphy, S. M., Permar, W., Hu, L., Campos, T. L., Hall, S. R., Ullmann, K., Zhang,
957   X., Flocke, F., Fischer, E. V., and Thornton, J. A.: Quantification of organic aerosol and brown carbon evolution in
958   fresh wildfire plumes, Proc. Natl. Acad. Sci., 117, 29469–29477, https://doi.org/10.1073/pnas.2012218117, 2020.

959   Parrish, D. D., Holloway, J. S., and Fehsenfeld, F. C.: Routine, Continuous Measurement of Carbon Monoxide with
960   Parts per Billion Precision, Environ. Sci. Technol., https://doi.org/10.1021/es00058a013, 1994.

961   Patashnick, H. and Rupprecht, E. G.: Continuous PM-10 Measurements Using the Tapered Element Oscillating
962   Microbalance, J. Air Waste Manage. Assoc., 41, 1079–1083, https://doi.org/10.1080/10473289.1991.10466903,
963   1991.

964   Permar, W., Wang, Q., Selimovic, V., Wielgasz, C., Yokelson, R. J., Hornbrook, R. S., Hills, A. J., Apel, E. C., Ku,
965   I., Zhou, Y., Sive, B. C., Sullivan, A. P., Collett, J. L., Campos, T. L., Palm, B. B., Peng, Q., Thornton, J. A.,
966   Garofalo, L. A., Farmer, D. K., Kreidenweis, S. M., Levin, E. J. T., DeMott, P. J., Flocke, F., Fischer, E. V., and Hu,
967   L.: Emissions of Trace Organic Gases From Western U.S. Wildfires Based on WE-CAN Aircraft Measurements, J.
968   Geophys. Res. Atmos., 126, https://doi.org/10.1029/2020JD033838, 2021.

969   Pratt, K. A., Murphy, S. M., Subramanian, R., Demott, P. J., Kok, G. L., Campos, T., Rogers, D. C., Prenni, A. J.,
970   Heymsfield, A. J., Seinfeld, J. H., and Prather, K. A.: Flight-based chemical characterization of biomass burning
971   aerosols within two prescribed burn smoke plumes, Atmos. Chem. Phys., https://doi.org/10.5194/acp-11-12549-
972   2011, 2011.

973   Prichard, S. J., O'Neill, S. M., Eagle, P., Andreu, A. G., Drye, B., Dubowy, J., Urbanski, S., and Strand, T. M.:
974   Wildland fire emission factors in North America: synthesis of existing data, measurement needs and management
975   applications, Int. J. Wildl. Fire, 29, 132, https://doi.org/10.1071/WF19066, 2020.

976   Reid, C. E., Brauer, M., Johnston, F. H., Jerrett, M., Balmes, J. R., and Elliott, C. T.: Critical Review of Health
977   Impacts of Wildfire Smoke Exposure, Environ. Health Perspect., 124, 1334–1343,
978   https://doi.org/10.1289/ehp.1409277, 2016.

979   Saleh, R., Hennigan, C. J., McMeeking, G. R., Chuang, W. K., Robinson, E. S., Coe, H., Donahue, N. M., and
980   Robinson, A. L.: Absorptivity of brown carbon in fresh and photo-chemically aged biomass-burning emissions,
981   Atmos. Chem. Phys., 13, 7683–7693, https://doi.org/10.5194/acp-13-7683-2013, 2013.

982   Schroeder, W. and Giglio, L.: NASA VIIRS Land Science Investigator Processing System (SIPS) Visible Infrared
983   Imaging Radiometer Suite (VIIRS) 375 m & 750 m Active Fire Products: Product User's Guide, Nasa, 1.4, 2–23,
984   2018.

985   Selimovic, V., Yokelson, R. J., McMeeking, G. R., and Coefield, S.: In situ measurements of trace gases, PM, and
986   aerosol optical properties during the 2017 NW US wildfire smoke event, Atmos. Chem. Phys., 19, 3905–3926,

987   https://doi.org/10.5194/acp-19-3905-2019, 2019.

988   Shamarock, W. C., Klemp, J. B., Dudhia, J., Gill, D. O., Liu, Z., Berner, J., Wang, W., Powers, J. G., Duda, M. G.,

989   Barker, D. M., and Huang, X.-Y.: A Description of the Advanced Research WRF Model Version 4,

990   https://doi.org/10.5065/1DFH-6P97, 2019.

991   Singleton, M. P., Thode, A. E., Sánchez Meador, A. J., and Iniguez, J. M.: Increasing trends in high-severity fire in

992   the southwestern USA from 1984 to 2015, For. Ecol. Manage., 433, 709–719,

993   https://doi.org/10.1016/j.foreco.2018.11.039, 2019.

994   Sinha, P., Hobbs, P. V., Yokelson, R. J., Bertschi, I. T., Blake, D. R., Simpson, I. J., Gao, S., Kirchstetter, T. W., and

995   Novakov, T.: Emissions of trace gases and particles from savanna fires in southern Africa, J. Geophys. Res. Atmos.,

996   108, https://doi.org/10.1029/2002JD002325, 2003.

997   Stein, A. F., Draxler, R. R., Rolph, G. D., Stunder, B. J. B., Cohen, M. D., and Ngan, F.: NOAA's HYSPLIT

998   Atmospheric Transport and Dispersion Modeling System, Bull. Am. Meteorol. Soc., 96, 2059–2077,

999   https://doi.org/10.1175/BAMS-D-14-00110.1, 2015.

1000   Strand, T., Gullett, B., Urbanski, S., O'Neill, S., Potter, B., Aurell, J., Holder, A., Larkin, N., Moore, M., and Rorig,

1001   M.: Grassland and forest understorey biomass emissions from prescribed fires in the south-eastern United States -

1002   RxCADRE 2012, Int. J. Wildl. Fire, https://doi.org/10.1071/WF14166, 2016.

1003   Sullivan, A. P., Pokhrel, R. P., Shen, Y., Murphy, S. M., Toohey, D. W., Campos, T., Lindaas, J., Fischer, E. V., and

1004   Collett Jr., J. L.: Examination of brown carbon absorption from wildfires in the western US during the WE-CAN

1005   study, Atmos. Chem. Phys., 22, 13389–13406, https://doi.org/10.5194/acp-22-13389-2022, 2022.

1006   Travis, K. R., Crawford, J. H., Soja, A. J., Gargulinski, E. M., Moore, R. H., Wiggins, E. B., Diskin, G. S., DiGangi,

1007   J. P., Nowak, J. B., Halliday, H., Yokelson, R. J., McCarty, J. L., Simpson, I. J., Blake, D. R., Meinardi, S.,

1008   Hornbrook, R. S., Apel, E. C., Hills, A. J., Warneke, C., Coggon, M. M., Rollins, A. W., Gilman, J. B., Womack, C.

1009   C., Robinson, M. A., Katich, J. M., Peischl, J., Gkatzelis, G. I., Bourgeois, I., Rickly, P. S., Lamplugh, A., Dibb, J.

1010   E., Jimenez, J. L., Campuzano-Jost, P., Day, D. A., Guo, H., Pagonis, D., Wennberg, P. O., Crounse, J. D., Xu, L.,

1011   Hanisco, T. F., Wolfe, G. M., Liao, J., St. Clair, J. M., Nault, B. A., Fried, A., and Perring, A. E.: Emission Factors

1012   for Crop Residue and Prescribed Fires in the Eastern US During FIREX-AQ, J. Geophys. Res. Atmos., 128,

1013   https://doi.org/10.1029/2023JD039309, 2023.

1014   USDA: Wildfire crisis strategy implementation plan: A 10-year implementation plan, 1–11, 2022.

1015   Virkkula, A., Ahlquist, N. C., Covert, D. S., Arnott, W. P., Sheridan, P. J., Quinn, P. K., and Coffman, D. J.:

1016   Modification, calibration and a field test of an instrument for measuring light absorption by particles, Aerosol Sci.

1017   Technol., https://doi.org/10.1080/027868290901963, 2005.

1018   Virkkula, A., Mäkelä, T., Hillamo, R., Yli-Tuomi, T., Hirsikko, A., Hämeri, K., and Koponen, I. K.: A Simple

1019   Procedure for Correcting Loading Effects of Aethalometer Data, J. Air Waste Manage. Assoc., 57, 1214–1222,

1020 https://doi.org/10.3155/1047-3289.57.10.1214, 2007.

1021 Wang, J., Yue, Y., Wang, Y., Ichoku, C., Ellison, L., and Zeng, J.: Mitigating Satellite-Based Fire Sampling
1022 Limitations in Deriving Biomass Burning Emission Rates: Application to WRF-Chem Model Over the Northern
1023 sub-Saharan African Region, J. Geophys. Res. Atmos., https://doi.org/10.1002/2017JD026840, 2018.

1024 Warneke, C., Schwarz, J. P., Dibb, J., Kalashnikova, O., Frost, G., Al-Saad, J., Brown, S. S., Brewer, W. A., Soja,
1025 A., Seidel, F. C., Washenfelder, R. A., Wiggins, E. B., Moore, R. H., Anderson, B. E., Jordan, C., Yacovitch, T. I.,
1026 Herndon, S. C., Liu, S., Kuwayama, T., Jaffe, D., Johnston, N., Selimovic, V., Yokelson, R., Giles, D. M., Holben,
1027 B. N., Goloub, P., Popovici, I., Trainer, M., Kumar, A., Pierce, R. B., Fahey, D., Roberts, J., Gargulinski, E. M.,
1028 Peterson, D. A., Ye, X., Thapa, L. H., Saide, P. E., Fite, C. H., Holmes, C. D., Wang, S., Coggon, M. M., Decker, Z.
1029 C. J., Stockwell, C. E., Xu, L., Gkatzelis, G., Aikin, K., Lefer, B., Kaspari, J., Griffin, D., Zeng, L., Weber, R.,
1030 Hastings, M., Chai, J., Wolfe, G. M., Hanisco, T. F., Liao, J., Campuzano Jost, P., Guo, H., Jimenez, J. L., and
1031 Crawford, J.: Fire Influence on Regional to Global Environments and Air Quality (FIREX-AQ), J. Geophys. Res.
1032 Atmos., 128, https://doi.org/10.1029/2022JD037758, 2023.

1033 Wyden, R. and Manchin, J.: National Prescribed Fire Act of 2020, , 116TH CONGRESS. 2D SESSION, 2020.

1034 Xi, Y., Kshirsagar, A. V., Wade, T. J., Richardson, D. B., Brookhart, M. A., Wyatt, L., and Rappold, A. G.:
1035 Mortality in US Hemodialysis Patients Following Exposure to Wildfire Smoke, J. Am. Soc. Nephrol., 31, 1824–
1036 1835, https://doi.org/10.1681/ASN.2019101066, 2020.

1037 Xiu, M., Jayaratne, R., Thai, P., Christensen, B., Zing, I., Liu, X., and Morawska, L.: Evaluating the applicability of
1038 the ratio of PM2.5 and carbon monoxide as source signatures, Environ. Pollut., 306, 119278,
1039 https://doi.org/10.1016/j.envpol.2022.119278, 2022.

1040 Yan, J., Wang, X., Gong, P., Wang, C., and Cong, Z.: Review of brown carbon aerosols: Recent progress and
1041 perspectives, Sci. Total Environ., 634, 1475–1485, https://doi.org/10.1016/j.scitotenv.2018.04.083, 2018.

1042 Yokelson, R. J., Goode, J. G., Ward, D. E., Susott, R. A., Babbitt, R. E., Wade, D. D., Bertschi, I., Griffith, D. W.
1043 T., and Hao, W. M.: Emissions of formaldehyde, acetic acid, methanol, and other trace gases from biomass fires in
1044 North Carolina measured by airborne Fourier transform infrared spectroscopy, J. Geophys. Res. Atmos., 104,
1045 30109–30125, https://doi.org/10.1029/1999JD900817, 1999.

1046 Yokelson, R. J., Burling, I. R., Gilman, J. B., Warneke, C., Stockwell, C. E., De Gouw, J., Akagi, S. K., Urbanski, S.
1047 P., Veres, P., Roberts, J. M., Kuster, W. C., Reardon, J., Griffith, D. W. T., Johnson, T. J., Hosseini, S., Miller, J.
1048 W., Cocker, D. R., Jung, H., and Weise, D. R.: Coupling field and laboratory measurements to estimate the emission
1049 factors of identified and unidentified trace gases for prescribed fires, Atmos. Chem. Phys.,
1050 https://doi.org/10.5194/acp-13-89-2013, 2013.

1051 Yu, Y., Zou, W., Jerrett, M., and Meng, Y.-Y.: Acute health impact of wildfire-related and conventional PM2.5 in
1052 the United States: A narrative review, Environ. Adv., 12, 100179, https://doi.org/10.1016/j.envadv.2022.100179,

1053   2023.

1054   Zeng, L., Dibb, J., Scheuer, E., Katich, J. M., Schwarz, J. P., Bourgeois, I., Peischl, J., Ryerson, T., Warneke, C.,

1055   Perring, A. E., Diskin, G. S., DiGangi, J. P., Nowak, J. B., Moore, R. H., Wiggins, E. B., Pagonis, D., Guo, H.,

1056   Campuzano-Jost, P., Jimenez, J. L., Xu, L., and Weber, R. J.: Characteristics and evolution of brown carbon in

1057   western United States wildfires, Atmos. Chem. Phys., 22, 8009–8036, https://doi.org/10.5194/acp-22-8009-2022,

1058   2022.

1059   Zhong, M. and Jang, M.: Dynamic light absorption of biomass-burning organic carbon photochemically aged under

1060   natural sunlight, Atmos. Chem. Phys., 14, 1517–1525, https://doi.org/10.5194/acp-14-1517-2014, 2014.

1061

1062

Tables

Table 1. The $PM_{2.5}$ mass, BC, and BrC NEMRs relative to CO (based on regression slopes) and coefficients of determination (r^2) in the column to the right of each NEMR for the smoke events identified in this study*.

Smoke event Date/Trailer	NEMR $PM_{2.5}$ mass ($\mu g\ m^{-3}\ ppb^{-1}$)	r^2	NEMR $PM_{2.5}$ BC ($\mu g\ m^{-3}\ ppb^{-1}$)	r^2	NEMR $PM_{2.5}$ BrC ($\mu g\ m^{-3}\ Mm^{-1}$)	r^2	Age estimated by wind vector (min)	Age estimated by HYSPLIT (min)
3/23/21 T Main	0.125	0.66	0.010	0.74	0.257	0.59	108	40
4/06/21 T Main	0.097	0.90	0.012	0.96	0.187	0.82	75	130
4/07/21 T Main	0.160	0.90	0.012	0.93	0.367	0.86	14	10
4/08/21 T Main	0.105	0.90	0.005	0.84	0.199	0.85	162	40
4/14/21 T Main	0.146	0.72	0.015	0.76	0.324	0.61	44	20
4/20/21 T Main	0.080	0.74	0.011	0.83	0.151	0.63	5	10
4/21/21 T Main	0.107	0.75	0.009	0.90	0.133	0.70	330	190
4/30/21 T Main	0.141	0.94	0.007	0.95	0.319	0.87	-	-
2/11/22 T Main	0.054	0.93	0.022	0.95	0.567	0.95	8	10
2/12/22 T Main	0.066	0.82	0.018	0.96	0.514	0.93	60	50
2/13/22 T Main	0.053	0.81	0.016	0.83	0.613	0.85	26	20
2/13/22 T Main	0.042	0.86	0.014	0.89	0.689	0.85	30	20
2/26/22 T Main	0.207	0.88	0.018	0.98	0.690	0.97	130	110
2/27/22 T Main	0.119	0.70	0.010	0.87	0.334	0.91	-	-
3/01/22 T Main	0.166	0.81	0.016	0.91	0.586	0.94	92	270
3/02/22 T Main	0.129	0.75	0.020	0.87	0.608	0.87	60	40
3/04/22 T Main	0.209	0.69	0.005	0.53	0.167	0.92	-	160
3/04/22 T Main	0.121	0.89	0.012	0.98	0.454	0.97	-	40
3/07/22 T Main	0.122	0.82	0.009	0.96	0.405	0.96	224	-
3/07/22 T Main	0.170	0.66	0.012	0.97	0.338	0.89	-	10
3/14/22 T Main	0.138	0.82	0.010	0.93	0.575	0.88	-	20
3/25/22 T Main	0.090	0.78	0.009	0.86	0.375	0.91	5	10
3/29/22 T Main	0.121	0.68	0.008	0.68	0.420	0.76	5	10
4/04/22 T Main	0.129	0.90	0.009	0.96	0.551	0.92	168	130
4/25/22 T Main	0.283	0.83	0.022	0.91	1.382	0.77	169	90
5/09/22 T Main	0.237	0.96	0.008	0.94	0.324	0.94	330	150
3/21/22 T 1293	0.188	0.98	-	-	-	-	89	20
3/25/22 T 1293	0.158	0.93	-	-	-	-	45	30
3/26/22 T 1293	0.148	0.97	-	-	-	-	5	10
3/27/22 T 1293	0.176	0.84	-	-	-	-	5	10
3/28/22 T 1293	0.129	0.81	-	-	-	-	-	60
3/29/22 T 1293	0.093	0.87	-	-	-	-	-	210
4/05/22 T 1293	0.277	0.91	0.016	0.78	0.280	0.47	-	360
4/21/22 T 1293	0.466	0.98	0.024	0.83	1.55	0.48	78	-
4/23/22 T 1293	0.121	0.59	0.013	0.80	0.317	0.33	28	10
4/23/22 T 1293	0.165	0.97	0.014	0.96	0.354	0.94	48	10
4/24/22 T 1293	0.248	0.90	-	-	-	-	63	40
4/26/22 T 1293	0.182	0.96	-	-	-	-	106	-
5/09/22 T 1293	0.238	0.99	0.012	0.98	0.321	0.94	480	210
5/10/22 T 1293	0.112	0.92	0.008	0.83	0.406	0.78	474	160
5/11/22 T 1293	0.168	0.77	-	-	-	-	5	10
5/12/22 T 1293	0.119	0.94	-	-	-	-	5	10
5/09/22 T 1291	0.265	0.98	-	-	-	-	296	160

* The table lists all events where both $PM_{2.5}$ mass and CO concentration were both available. In some cases BC and BrC data was not available and left as blank values (-).
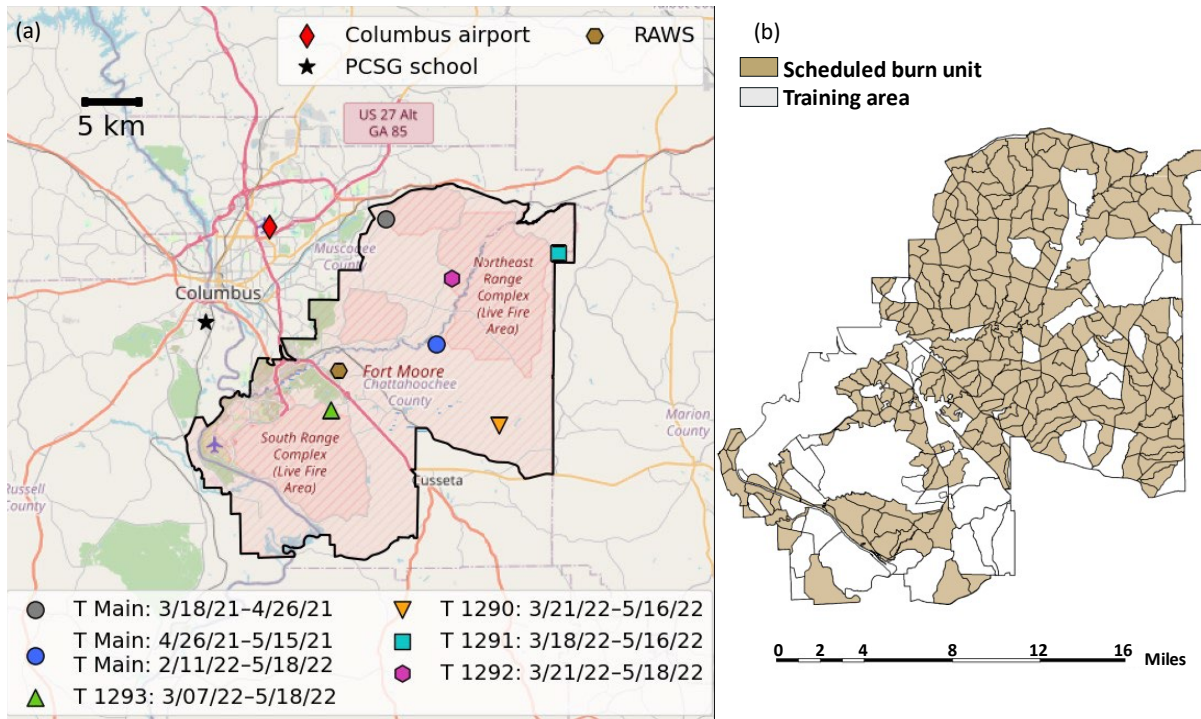
Figures



1070

Figure 1. Study region overview. (a) Fort Moore map with the locations of trailers, RAWS weather station, and two state-operated sampling sites, Columbus Airport and Phenix City South Girard (PCSG) school, are shown along with the location of the city of Columbus GA. (b) Fort Moore map showing the planned burn units for the year 2021, sourced from Fort Moore authorities and natural resources management team, with prevailing winds in the region.

1075
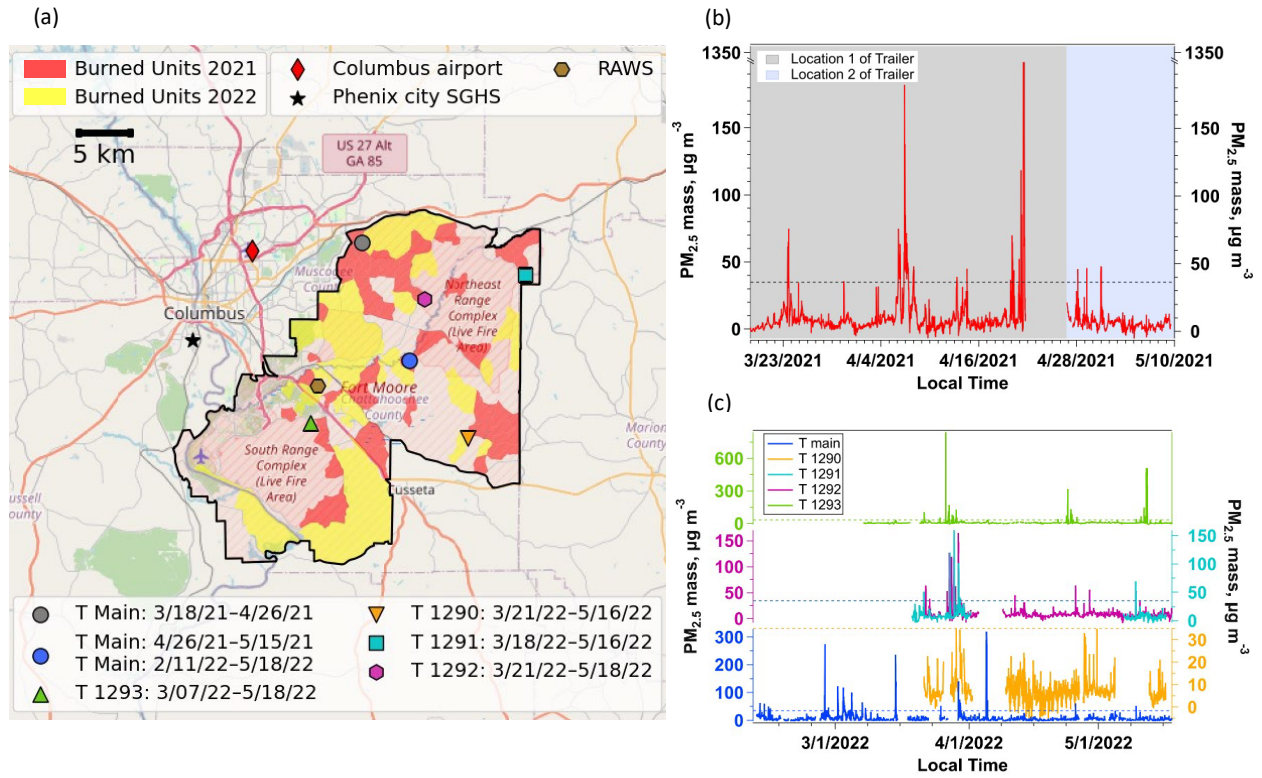
Figure 2. $PM_{2.5}$ mass measurements over two burning years. (a) Map of the burnt areas in the years 2021 and 2022 and locations of monitoring sites. (b) Time series of 20-minutes average $PM_{2.5}$ mass concentration measured at the main trailer during the burning season of 2021, and (c) 2022 across different sites. Dotted lines represent $PM_{2.5}$ mass concentration of 35 µg m^{-3} above which peaks were selected for detailed analysis.

1084

1085
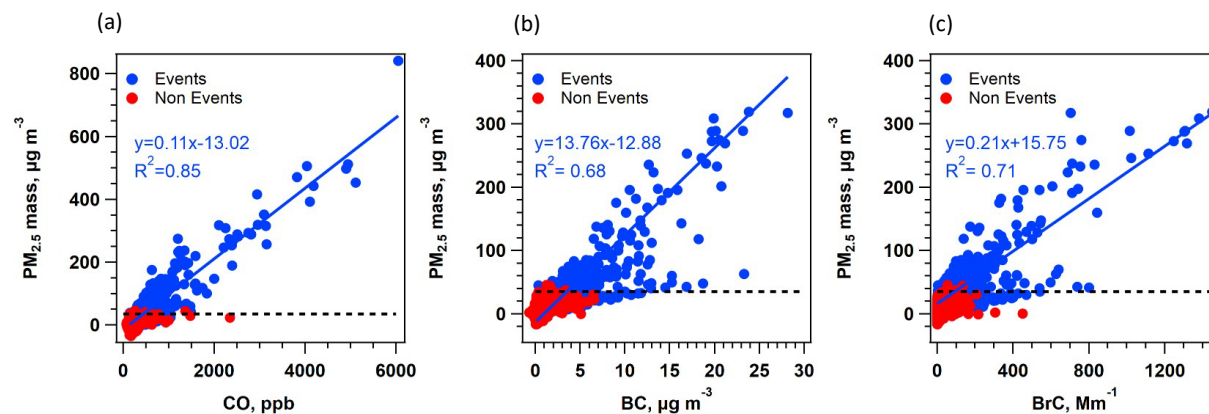
Figure 3. Correlations between $PM_{2.5}$ mass concentration and CO, $PM_{2.5}$ BC, and $PM_{2.5}$ BrC for measurements from the main trailer in 2021 and 2022 and T1291 and T1293 in 2022. Blue data points are characterized as $PM_{2.5}$ events when the concentration is > 35 $\mu g\ m^{-3}$ averaged over a 20-minute period. In the plot all data associated with an identified event is shown as blue (This includes event data down to the background levels before and after the peak). All other data (non-events) are shown in red. Slope is from orthogonal distance regression (ODR) of the 20-minute averaged data during events periods.

1092

1093
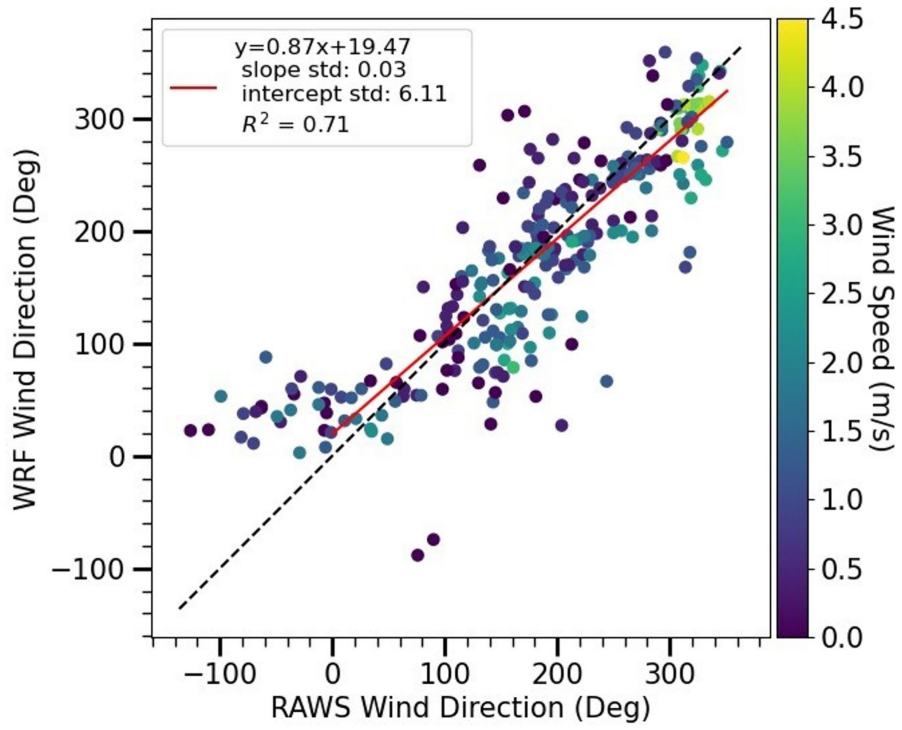
1094

Figure 4. Comparison between wind direction modeled via WRF versus that recorded by the RAWS located at Fort Moore. Slope is from orthogonal distance regression (ODR).

1097

1098

1099
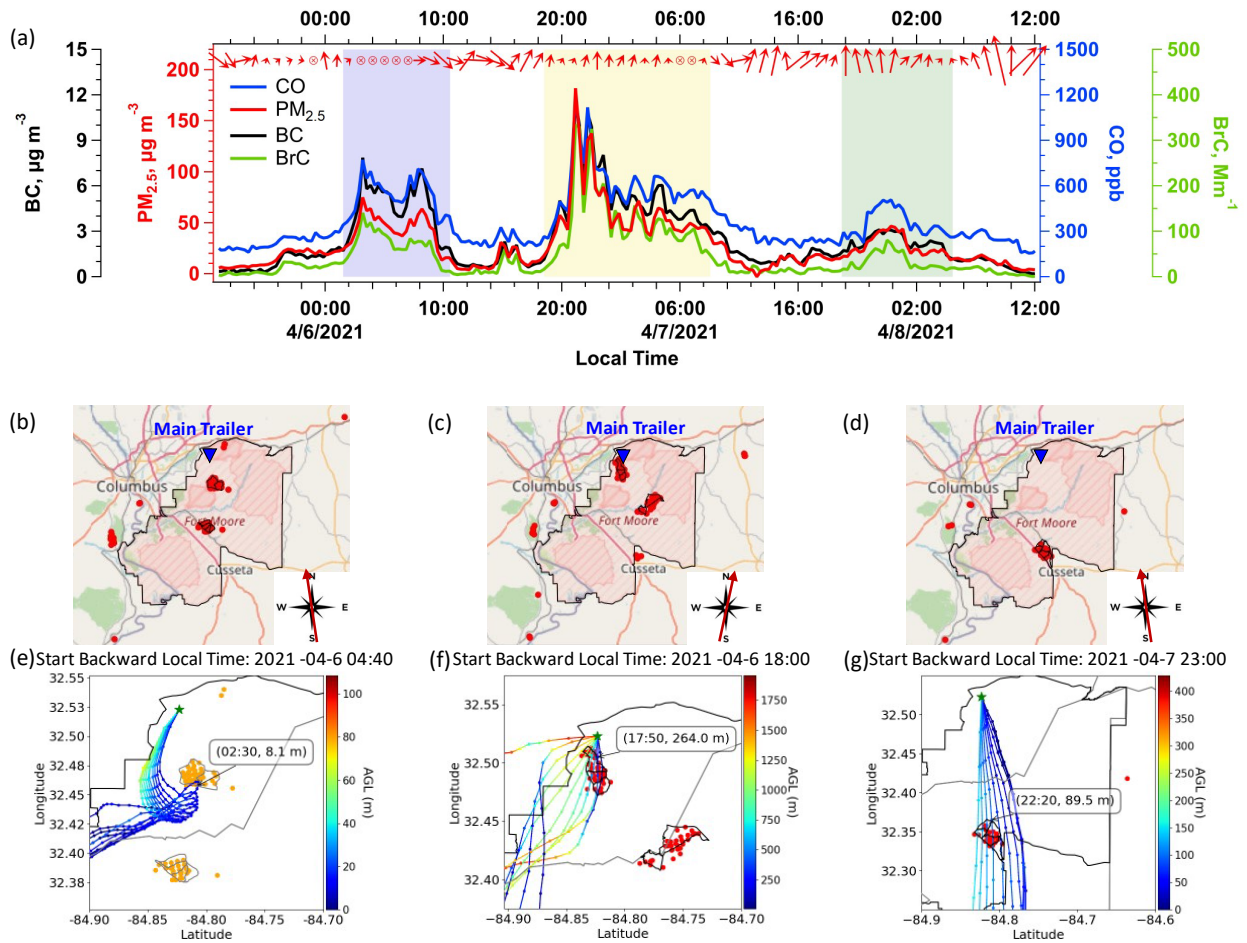
Figure 5. Three case studies illustrating the application of our method in determining the source of smoke events. (a) Time series of species measured at the main trailer. Time resolution is 20 minutes for CO, PM$_{2.5}$ mass, BC, and BrC. The wind vectors depict hourly data obtained from RAWS, with the direction of the arrow indicating wind direction, and the length of the arrow representing wind speed. (b,c,d) Maps of the Fort showing historical satellite data from the FIRMS website observed for April 5, 6, and 7, 2022. Red dots represent fires detected by the satellite. (e,f,g) Are HYSPLIT back trajectories during the occurrence of each of the three peaks. Date and time of the backward trajectory is indicated on top of each map. Time and height at which the trajectory crosses the trailer is shown in the box inside each map. Red dots are fires detected by FIRMS the same day of the backward trajectory. Orange dots are fires detected by FIRMS one day before the day of the backward trajectory. The colors of the traces in the back trajectories indicate the height above ground level. Green star marks the location of the main trailer. Satellite overpasses times are shown in Table S9.

1110

1111

(a)

WRF Wind Speed, ms^{-1}

ODR:

y=1.84x+0.93 (R^2=0.29)

● Day
● Night

RAWS Wind Speed, ms^{-1}

(b)

HYSPLIT Age, min

ODR:

y=0.46x+15.55 (R^2=0.59)

Zero-intercept regression:

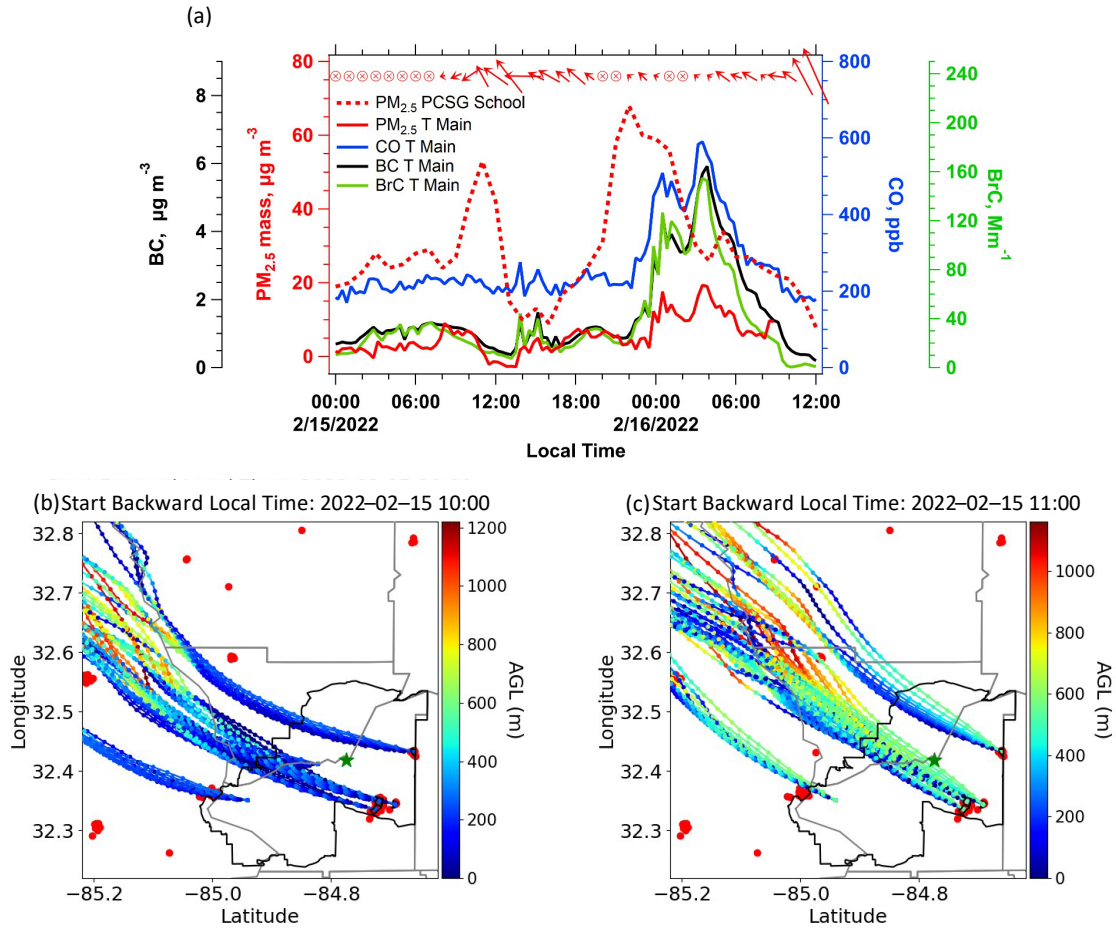y=0.49x (R^2=0.85)

Wind Vector Age, min
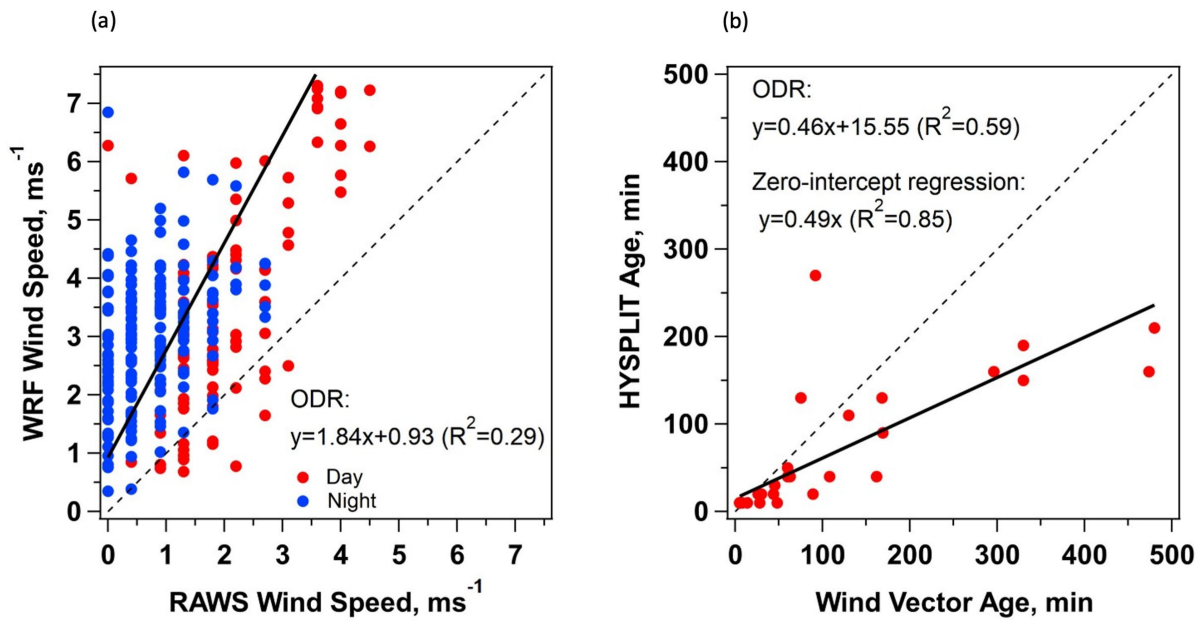
1112

1113   **Figure 6.** (a) Comparison between wind speed modeled via WRF versus that observed by RAWS located on Fort Moore. (b)
1114   Comparison between age estimated using HYSPLIT model versus the wind vector method.

1115

(a)

(b) Start Backward Local Time: 2022–02–15 10:00

(c) Start Backward Local Time: 2022–02–15 11:00

Figure 7. Case study of missing smoke at monitoring site despite expectations according to wind direction. (a) Time series of species measured at the main trailer. Time resolution is 20 minutes for CO, PM$_{2.5}$ mass, BC, and BrC. The wind vectors depict hourly data sourced from RAWS, with the direction of the arrow indicating wind direction, and the length of the arrow representing wind speed. Data from PCSG school are hourly averages; (b, c) HYSPLIT forward trajectories starting from the two prescribed fires on the base on February 15, 2022 at 10:00 and 11:00, respectively. Red dots are fires detected on FIRMS the same day (satellite overpass happened on February 15, 2022 at 12:54, 13:49, 14:32, and 14:36).

1125
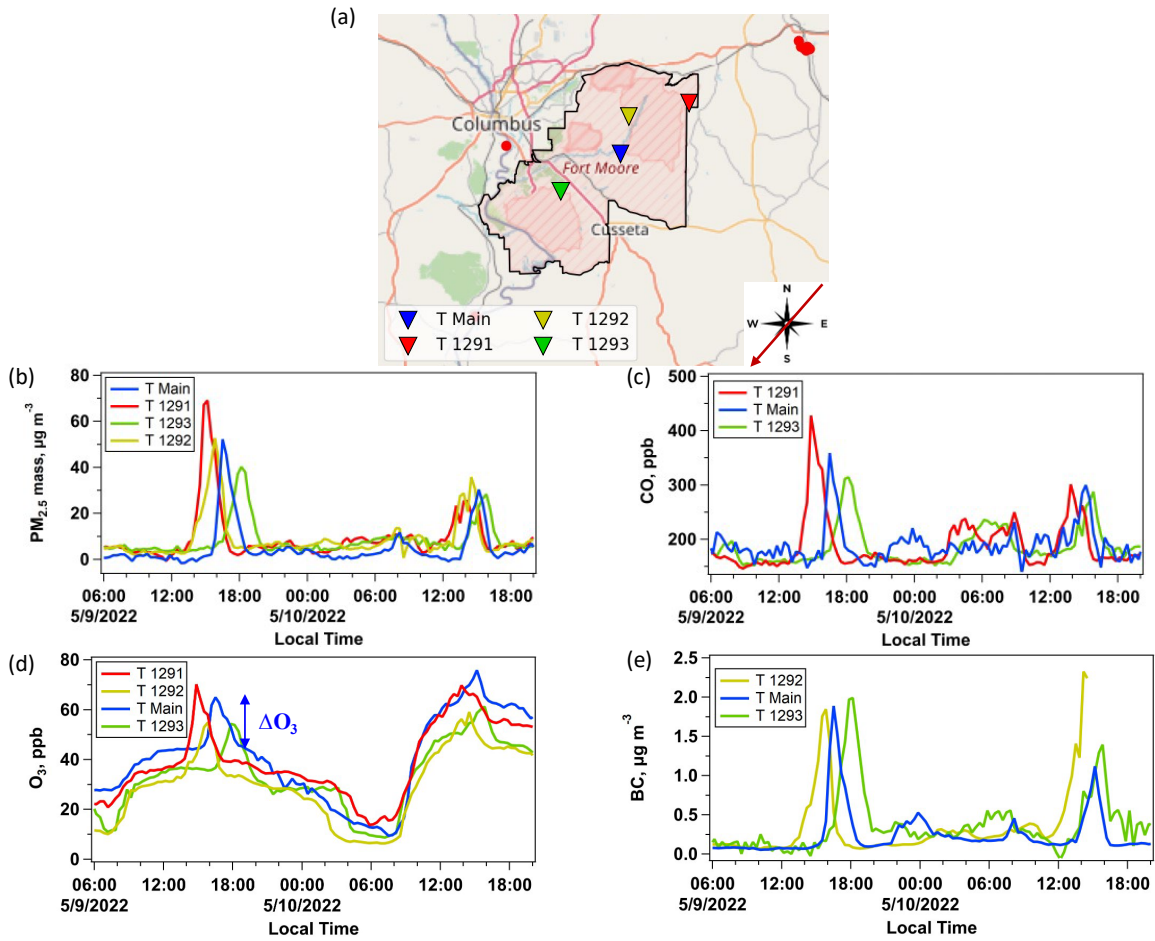
1126

1127 **Figure 8.** Case study of smoke detection sequentially at 4 monitoring trailers. (a) Map of the Fort showing historical satellite data
1128 from the FIRMS website observed for May 9, 2022 (satellite overpass happened on May 9, 2022 at 12:38, 13:54, and 14:42) and
1129 average wind vector from 13:00 to 16:00 local time. Time series showing 20 minutes data of (b) PM$_{2.5}$ mass and (c) CO on main
1130 trailer, (d) O$_3$ concentration, and (e) BC concentration for, main trailer, T1291, T1292, and T1293. Note that no CO instrument was
1131 operating at T1292 and no BC data for T1291.

1132

1133
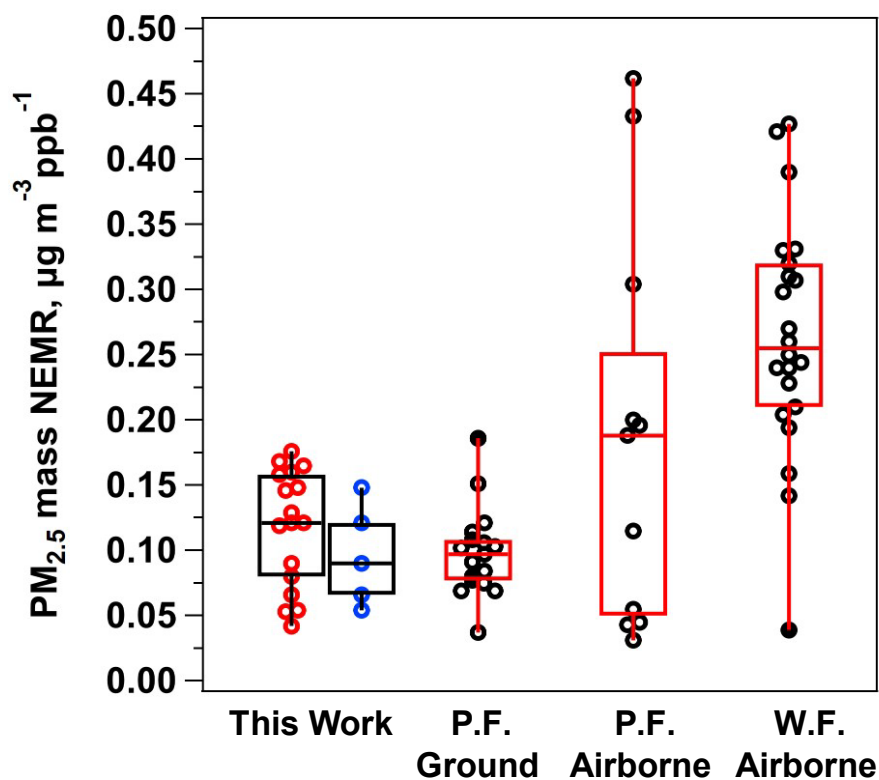
1134

1135 **Figure 9.** Box plot of $PM_{2.5}$ mass NEMRs of smoke events of estimated age ≤ 1 hour in this study in comparison to other studies.
1136 Blue symbols are smoke plumes with observed O_3 enhancements. The horizontal line inside the box represents the median of the
1137 data. The top line of the box represents the third quartile (Q3), and the bottom line represents the first quartile (Q1). Colored circles
1138 represent data outliers. P. F. is Prescribed Fires, W.F. is wildfires. Some of the emission ratios reported in literature and included
1139 in the plot correspond to ΔOA/ΔCO since OA tends to dominate $\Delta PM_{2.5}$ mass concentration (see Table S10).

1140

1141
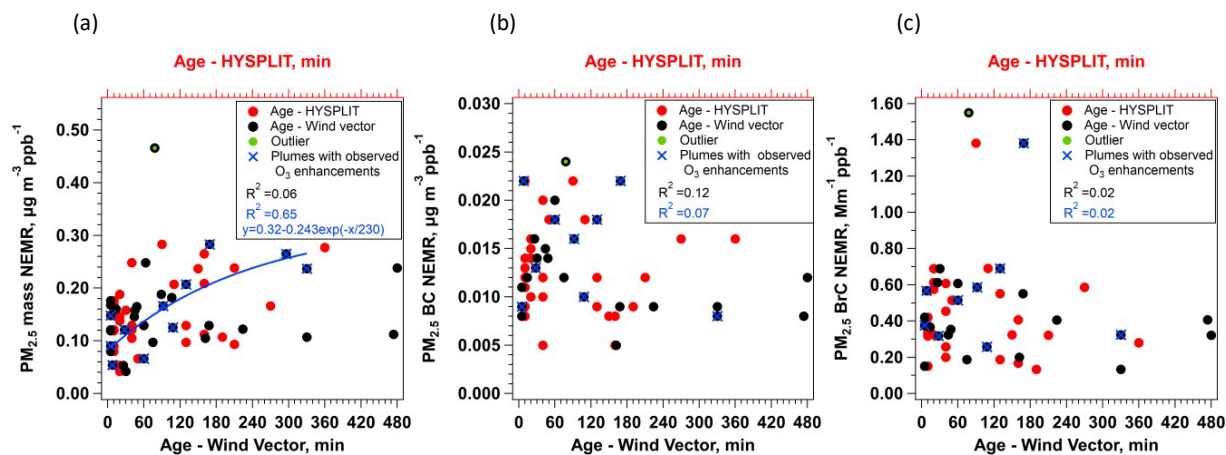
1142

1143 **Figure 10.** (a) PM$_{2.5}$ mass, (b) BC, and (c) BrC NEMRs of all studied smoke events as a function of age estimated using average
1144 wind vector and HYSPLIT analysis. Smoke plumes with observed O$_3$ enhancements are identified. Linear regression coefficients
1145 of determination (r^2) for all data and for just O$_3$ enhancement periods are identified. The exponential fit equation for PM$_{2.5}$ mass
1146 NEMRs for O$_3$ enhancement periods is shown in (a).

1147

44

1148
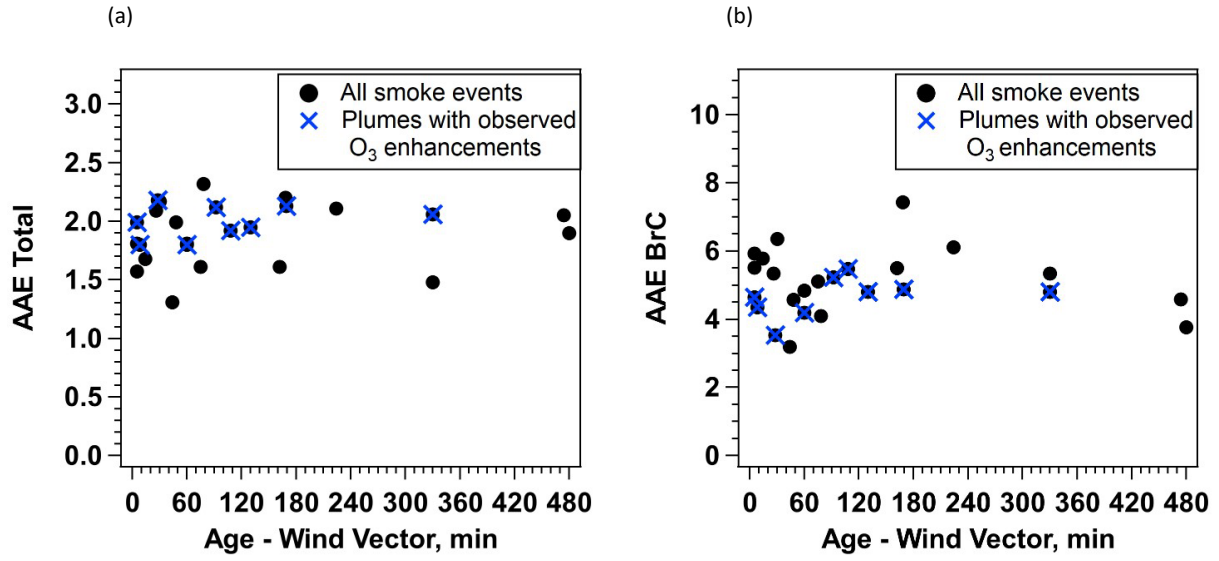
1149

1150 **Figure 11.** Average AAE values for a) total light absorption (BC+BrC) and b) BrC species for all smoke events for which
1151 aethalometer data is available. Smoke plumes with observed O_3 enhancements are identified.

1152

1153

1154

1155

1156

1157